miR-146a-5p mediates inflammation-induced β cell mitochondrial dysfunction and apoptosis

Preethi Krishnan[1,2,3], Renato Chaves Souto Branco[2,3,4], Staci A. Weaver[2,3,5], Garrick Chang[6], Chih-Chun Lee,[2,3,4], Farooq Syed[2,3,4] *, and Carmella Evans-Molina[1,2,3,4,7] *

Department of [1]Medicine, [2]Herman B Wells Center for Pediatric Research, [3]Center for Diabetes and Metabolic Diseases, Departments of [4]Pediatrics, [5]Biochemistry and Molecular Biology, and [6]Physics, Indiana University School of Medicine, and [7]Roudebush VA Medical Center, Indianapolis, IN 46202, USA

Running Title: ***miR-146a-5p regulates β cell mitochondrial health***

***To whom correspondence should be addressed**:
Carmella Evans-Molina, MD, Ph.D., Indiana University School of Medicine, 635 Barnhill Drive MS 2031A, Indianapolis, IN, USA; Tel: (317) 274-4145, Fax: (317) 274-4107, email: cevansmo@iu.edu or Farooq Syed, PhD., Indiana University School of Medicine, 635 Barnhill Drive MS 2055, Indianapolis, IN, USA; Tel: (317) 278-9517, email: fsyed@iupui.edu

Keywords: microRNA, miR-146a-5p, diabetes, mitochondrial function, β cell, insulin, pancreatic islets, MIN6 cells, diabetes

ABSTRACT

We previously showed that miR-146a-5p is upregulated in pancreatic islets treated with pro-inflammatory cytokines. Others have reported that miR-146a-5p overexpression is associated with β cell apoptosis and impaired insulin secretion. However, the molecular mechanisms mediating these effects remain elusive. To investigate the role of miR-146a-5p in β cell function, we developed stable MIN6 cell lines to either overexpress or inhibit the expression of miR-146a-5p. Monoclonal cell populations were treated with pro-inflammatory cytokines (IL-1β, IFNγ, and TNFα) to model T1D *in vitro*. We found that overexpression of miR-146a-5p increased cell death under conditions of inflammatory stress, whereas inhibition of miR-146a-5p reversed these effects. Additionally, inhibition of miR-146a-5p increased mitochondrial DNA copy number, respiration rate, and ATP production. Further, RNA sequencing data showed enrichment of pathways related to insulin secretion, apoptosis, and mitochondrial function when the expression levels of miR-146a-5p were altered. Finally, a temporal increase in miR-146a-5p expression levels and a decrease in mitochondria function markers was observed in islets derived from NOD mice. Collectively, these data suggest that miR-146a-5p may promote β cell dysfunction and death during inflammatory stress by suppressing mitochondrial function.

INTRODUCTION

Type 1 diabetes (T1D) is characterized by immune-mediated destruction of pancreatic β cells and manifests clinically after a substantial loss of β cell mass and function, leading to severe hyperglycemia and metabolic instability (1). Evidence from clinical studies suggests that β cell loss may begin years before clinical diagnosis, and disease initiation is documented by the development of autoantibodies against β cell antigens, such as GAD, insulin, IA-2, and ZnT8 (2). Evidence from birth cohort studies shows that 85% of individuals positive for two or more autoantibodies will develop T1D within 15 years of follow-up (3).

Immune-mediated destruction of β cells in T1D is accompanied by the activation of a series of transcriptional and signaling pathways, which are thought to render the β cell more immunogenic while also invoking self-imposed dysfunction and/or death. Inflammatory insults such as pro-inflammatory cytokines contribute to T1D pathogenesis, and others have shown that treatment of mouse and human pancreatic islets and β cell lines with cytokines (IL1β, IFNγ, TNFα, IFNα) recapitulates many of the *in vivo* molecular changes seen in early and late stages of T1D (4, 5).

In addition to alterations in protein-coding genes, non-protein-coding genes, particularly microRNAs (miRNAs), contribute to T1D development (6–8). miRNAs are small non-coding RNAs that serve as global regulators of gene expression (9–11). miRNAs have been implicated in a variety of biological processes within the β cell, including endocrine cell specification (12), β cell development (13), insulin secretion (14), glucose regulation (15), and apoptosis (16). Previously, we identified miR-146a-5p as a cytokine-modulated miRNA in human islets treated with pro-inflammatory cytokines. miR-146a-5p was coordinately upregulated in human islets and islet-derived extracellular vesicles (6, 7). Notably, we observed an increase in expression of miR-146a-5p in plasma-derived extracellular vesicles from individuals with autoantibody-positivity and normoglycemia and in recent onset T1D, suggesting that miR-146a-5p may have utility as a T1D biomarker (7).

Previous research has demonstrated that robust and sustained upregulation of miR-146a-5p during inflammatory states led to an increase in apoptosis and a significant decrease in insulin secretion in MIN6 cells (17). However, the mechanisms through which miR-146a-5p exerts these effects remain elusive. Data from other inflammatory disease models show that miR-146a-5p has been classified as a mitomiR—a miRNA that is enriched in the mitochondria, where it is implicated to play a critical role in the regulation of mitochondrial function (18–20). Moreover, inflammation-mediated mitochondrial dysfunction has been established as a pivotal factor in the pathogenesis of T1D. (21–23). Our study aims to investigate whether miR-146a-5p contributes to T1D pathogenesis through dysregulation of mitochondrial function.

RESULTS

miR-146a-5p overexpression promotes β cell death under pro-inflammatory conditions

Our previous RNA sequencing analysis of human islets exposed to pro-inflammatory cytokines revealed a significant upregulation of miR-146a-5p during inflammation. (7). In agreement with these results, mouse islets (Fig. 1A) and MIN6 cells (Fig. 1B) that were exposed to pro-inflammatory cytokines (IL1β, IFNγ, and TNFα) for 24 hours showed a significant increase in the expression of miR-146a-5p. Next, to functionally delineate the role of miR-146a-5p in MIN6 cells, we established stable cell lines using a lentiviral vector. These included a lentiviral vector expressing a scrambled sequence with no similarity to any known mouse genomic sequence (Scr), a lentiviral vector overexpressing miR-146a-5p (OE), and a lentiviral vector with anti-sense miR-146a-5p (ZIP). qRT-PCR analysis of OE cells showed a significant upregulation of miR-146a-5p, while miR-146a-5p expression levels remained unchanged in cells transduced with the ZIP knockdown vector compared to Scr control (Fig. 1C). Furthermore, there was an

approximately 500-fold increase in miR-146a-5p levels in Scr cells treated with cytokines compared to untreated Scr cells (Fig. S1A). In contrast, we only observed a 2-fold increase in miR-146a-5p levels in ZIP cells treated with cytokines compared to untreated ZIP cells (Fig. S1B). Likewise, we observed an approximately 15-fold increase in miR-146a-5p levels in OE cells treated with cytokines compared to untreated OE cells (Fig. S1C).

To determine how modulation of miR-146a-5p levels impacts inflammation-mediated β cell death, we monitored cell death in real-time using a Sartorius Incucyte system. Exposure to pro-inflammatory cytokines increased cell death in wildtype MIN6 cells (without any vector; WT) and in Scr cells (Fig. 1D, Fig. S1D). Importantly, inhibition of miR-146a-5p expression (ZIP) reduced cell death in the presence of cytokines (Fig. 1E, Fig. S1E). Conversely, cell death was heightened in OE cells exposed to pro-inflammatory cytokines (Fig. 1F, Fig. S1F), suggesting a direct influence of miR-146a-5p on the regulation of β cell death and survival. Furthermore, we performed immunoblot to quantify the expression of total and cleaved caspase 3, a molecular marker of apoptosis. miR-146a-5p overexpression resulted in a pronounced increase in the cleaved-to-total caspase-3 ratio, whereas this elevation was largely mitigated in cytokine-treated MIN6 ZIP cells (Fig. S2).

miR-146a-5p regulates pathways related to β cell function and survival

To understand the impact of miR-146a-5p on gene expression, we performed bulk RNA sequencing on Scr, ZIP, and OE MIN6 cells treated with or without cytokines. After filtering for genes with a minimum of ten read counts in total, 17,696 genes were retained for downstream analysis. Principal component analysis (PCA) clustering of all the samples demonstrated distinct separation among the six experimental groups (Fig. 2A). Among all the experimental groups, OE and OE+Cy cells formed distinct clusters separated from the other groups. In contrast, ZIP and ZIP+Cy cells were clustered closer to the control (Scr) group.

First, to assess transcriptomic changes due to miR-146a-5p modulation, we compared ZIP and OE cells to Scr cells and identified 2,432 and 4,271 differentially expressed genes, respectively (Fig. 2B, Supplementary Tables S1a-S1b). Second, to identify genes that are differentially expressed as a result of pro-inflammatory stress, we compared Scr+Cy with Scr and identified 1,595 genes (Fig. 2B, Table S1c). Third, to test if there is a compounding effect of miR-146a-5p expression under inflammatory stress, we compared ZIP+Cy and OE+Cy with Scr as the control group and identified 3,537 and 5,655 genes as differentially expressed, respectively (Fig. 2B, Tables S1d-S1e).

Functional enrichment analysis was performed for differentially expressed genes identified from each comparison group. Applying the filtering criteria for gene ontology terms, we identified terms associated with insulin secretion, glucose, mitochondria, and endoplasmic reticulum, among others. Representative terms and a comparison of their fold enrichment values are provided in Fig. 2C. Notably, enrichment of terms related to mitochondria was observed across all comparison groups. For instance, the term "regulation of mitochondrial membrane potential" was enriched in ZIP vs. Scr and OE vs. Scr both in the presence and absence of cytokines. These findings suggest activation of pathways related to mitochondrial function under pro-inflammatory conditions, with miR-146a-5p potentially playing an independent role in the regulation of mitochondrial function. A complete list of functional terms for all the groups is provided in Supplementary Tables S2a-S2e.

miR-146a-5p exhibits enrichment in mitochondria during inflammatory stress

Next, to test if miR-146a-5p is enriched in mitochondria of MIN6 cells, we performed subcellular fractionation to isolate mitochondria and cytoplasm. ddPCR analysis from these fractions revealed that cytokine treatment led to

an increase in the copy number of miR-146a-5p in isolated cytoplasm (Fig. 3A) and mitochondria (Fig. 3B) of WT MIN6 cells. These results show that miR-146-5p is spatially located in both cytoplasm and mitochondria and that copy numbers increase under cytokine stress.

miR-146a-5p induces mitochondrial dysfunction

To assess the impact of miR-146a-5p modulation on mitochondrial function, we conducted several assays to evaluate mitochondrial metabolism, mitochondrial DNA copy number, mitochondrial ultrastructure and markers of mitochondrial function in MIN6 stable cells.

To detect differences in mitochondrial metabolism, we measured oxygen consumption rates (Fig. 3C) and individual respiratory parameters (Fig. 3D-3I) using the Seahorse XF Cell Mito Stress test in untreated and cytokine-treated Scr, ZIP, and OE cells. Scr group was used as the reference/control group for all comparisons. Our results indicate that ZIP cells exhibited higher basal respiratory rate, maximal respiration rate, and proton leak. Conversely, these parameters were reduced in OE cells upon cytokine treatment. Additionally, ATP production, and non-mitochondrial oxygen consumption rates were significantly lower in OE+Cy cells. These findings collectively suggest that inhibition of miR-146a-5p may partially improve mitochondrial respiratory activity.

We then quantified mitochondria DNA copy number in both cytokine-treated and untreated Scr, OE, and ZIP cells by quantifying the copy number of ND1, a mitochondria-encoded gene, relative to nuclear encoded genes *Tbp* and *Hprt*. Our analysis revealed a significant increase in ND1 in ZIP cells compared to Scr cells; in contrast, overexpression of miR-146a-5p did not induce any change in the copy number of ND1 compared to Scr (Fig. 4A).

Next, to assess whether the overexpression of miR-146a-5p induces ultrastructural changes in the β cells, we conducted transmission electron microscopy (TEM) microscopy analysis on the stable MIN6 cell lines. Under basal conditions, Scr cells exhibited normal mitochondrial architecture (Figure 4B). However, OE cells showed a potential reduction in the number of mitochondria, both in the presence and absence of pro-inflammatory cytokines (Fig. S3A). Furthermore, OE cells treated with cytokines exhibited a trend towards increased mitochondria perimeter (Fig. S3B), Feret's diameter (Fig. S3C), and aspect ratio (Fig. S3D), and a decrease in circularity (Fig. S3E) and roundness (Fig. S3F) compared to all the other groups. Conversely, the mitochondrial ultrastructure of ZIP cells remained unchanged by cytokine treatment, with an observed increase in the number of mitochondria in both ZIP and ZIP+Cy cells.

We then examined the expression pattern of an inner mitochondrial protein, TIM23, as a marker for mitochondrial function, in our stable MIN6 cell lines. In both the presence and absence of pro-inflammatory cytokines, cells overexpressing miR-146a-5p exhibited significantly lower levels of TIM23 protein compared to Scr and ZIP cells (Fig. 5). This reduction in TIM23 expression, even in the absence of cytokine treatment, suggests that overexpression of miR-146a-5p may drive mitochondrial dysfunction even under basal or unstressed conditions.

miR-146a-5p targets protein-coding genes related to insulin secretion, apoptosis, and mitochondrial function

Our results collectively indicate that miR-146a-5p is intricately involved in pathways crucial for β cell survival and function, potentially through modulation of mitochondrial function. To identify the gene targets through which these effects may be mediated, we predicted potential targets of miR-146a-5p using in silico analysis and overlapped these predictions with our RNA sequencing dataset, yielding 3,120 potential targets. Of these, 248 potential gene targets overlapped with genes identified from functional enrichment terms generated from all the comparisons (treated and untreated) from RNAseq analysis (shown in Fig.

2C). To narrow down this list of potential targets, we used several strategies: 1) we specifically focused on hits containing the terms "mitochondria," "cell death," "apoptosis," and "insulin," 2) to avoid considering genes that were altered because of cytokine exposure, we only considered differentially expressed genes in ZIP vs. Scr and OE vs. Scr comparisons, and 3) we only considered gene targets that showed opposite directions of expression in ZIP and OE cells. These strategies yielded a list of 102 potential gene targets. Of these, we chose 10 targets for further validation (Fig. 6), and qRT-PCR confirmed the differential expression of seven of these targets (*Brsk2*, *Eya1*, *Gpx1*, *Mapt*, *Myrip*, *Nrg1*, and *Perp*). *Myrip*, *Gpx1*, and *Nrg1* were upregulated in MIN6 ZIP cells under inflammatory stress, whereas *Brsk2* and *Eya1* were upregulated in cells overexpressing miR-146a-5p. In addition, the change in *Eya1* was significant in OE cells treated with cytokines. *Mapt* was downregulated and *Perp* was upregulated in OE cells treated with cytokines compared with all other groups. Notably, more than 60% of selected target genes were validated, highlighting the potential of miR-146a-5p to modulate novel pathways involved in β cell function and survival.

Islet mitochondrial dysfunction is observed in mouse models of T1D

To validate the presence of mitochondrial dysfunction in mouse models of T1D during disease progression, we performed immunofluorescence analysis to evaluate the expression of TIM23 and TOM20 (markers of mitochondria function), in islets isolated from nonobese diabetic (NOD) mice at various time points (7, 9, 11, and 13 weeks of age, Fig. 7A). We observed a decreasing trend in TOM20 expression (Fig. 7B) and a significant decrease in TIM23 expression in 13-week-old NOD mice (Fig. 7C), implying that islet mitochondrial function decreases during the progression to T1D. Concurrently, we examined the temporal expression of miR-146a-5p in isolated islets from NOD mice across various time points (5, 7, 9, 11, and 13 weeks of age). Our data demonstrated an elevation in miR-146a-5p expression (Fig. 7D) alongside the decrease in TIM23 and TOM20 expression levels, providing evidence of a correlation between increased miR-146a-5p expression and mitochondrial dysfunction.

DISCUSSION

In this study, we demonstrated that miR-146a-5p is upregulated under conditions of inflammatory stress and that its overexpression leads to mitochondrial dysfunction and apoptosis in β cells, which was reversed by inhibiting miR-146a-5p. These findings represent a novel insight into the role of miR-146a-5p in altering β cell health through the suppression of mitochondrial function.

We have shown previously that miR-146a-5p may serve as a circulating biomarker for T1D (7); however, the molecular mechanisms by which miR-146a-5p contributes to diabetes risk needed to be delineated. Roggli *et al*. demonstrated that prolonged exposure of β cells to palmitate and pro-inflammatory cytokines induced alterations in miR-146a-5p expression, including upregulation in human islets, MIN6 cells, and INS1 cells (17). Further, inhibition of miR-146a-5p improved glucose-stimulated insulin secretion and reduced apoptosis in cytokine-treated MIN6 cells. Our findings align with this study by Roggli *et al*., as we observed that overexpression of miR-146a-5p in the presence of pro-inflammatory cytokines led to increased apoptosis of MIN6 cells, suggesting that miR-146a-5p may be directly associated with β cell survival.

Functional enrichment analysis of differentially expressed genes identified through RNA sequencing in our MIN6 cell lines provides further insights into the role of miR-146a-5p in pathways associated with β cell survival and function. Notably, modulation of miR-146a-5p resulted in enrichment for terms related to mitochondria, including mitochondrial depolarization, mitochondrial organization, and apoptotic mitochondrial changes. These findings suggest a potential role for miR-146a-5p in T1D

pathogenesis, possibly through the modulation of mitochondrial function.

Mitochondria are directly associated with diabetes pathogenesis through alterations in oxidative phosphorylation, ATP production, reactive oxygen species (ROS) formation, and regulation of apoptosis (21–23). This association is supported by several lines of evidence from various studies, including observations of reduced mtDNA copy number in blood samples from individuals with type 2 diabetes (24) and decreased oxidative phosphorylation in the skeletal muscle of insulin-resistant offspring of individuals with T2D (25). Additionally, recent research has highlighted the involvement of miRNAs in mitochondrial function (19). For instance, Dasgupta *et al*. demonstrated the enrichment of miR-146a-5p in mitochondria and predicted mitochondrial genes such as *ND1*, *ND2*, *ND4*, *ND5*, *ND6*, and *ATP8* as potential targets of miR-146a-5p from 143B cell lines (18). In the context of diabetes, Zhen *et al*. reported a repertoire of mitochondria-associated miRNAs that were dysregulated in mouse liver upon streptozotocin-induced T1D (20). However, the presence and function of mitochondria-associated miRNA in pancreatic islets remain unclear.

To begin to understand if miR-146a-5p expression is detrimental to mitochondrial function, we showed that miR-146a-5p was enriched in mitochondria during inflammatory stress. In line with the observation, seahorse metabolic profiling demonstrated a significant increase in basal respiration, maximal respiration, spare respiratory capacity, proton leak, and ATP production upon inhibiting miR-146a-5p expression. However, these effects were reversed upon overexpressing miR-146a-5p, suggesting its involvement in inducing mitochondrial dysfunction by dampening the activity of the electron transport chain. Since mitochondrial morphology may play a role in metabolic activity (26), we assessed if there were ultrastructural changes in MIN6 stable cells. We observed a potential increase in mitochondria number in ZIP cells, whereas the number of mitochondria were decreased in OE cells treated with/without cytokines. Additionally, OE cells exhibited lower expression of TIM23 both in the presence or absence of cytokines. In a recent investigation, we reported that mitochondrial dysfunction, oxidative stress, and ER-stress pathways were prominently upregulated in prediabetic NOD mouse models (27). Furthermore, we identified 14 weeks of age in NOD mice as a critical point for the onset of T1D. Consistent with these findings, our current study reveals an inverse correlation between miR-146a-5p and TIM23 expression levels in islets from pre-diabetic female NOD mice across various time points. This finding suggests the potential involvement of miR-146a-5p in mitochondrial dysfunction during T1D progression.

To determine potential mechanisms underlying the impact of miR-146a-5p modulation on β cell function, we validated seven predicted gene targets of miR-146a-5p (*Brsk2*, *Eya1*, *Gpx1*, *Mapt*, *Myrip*, *Nrg1*, and *Perp*) via qRT-PCR in our stable MIN6 cell lines. Among these, *Brsk2* (BR Serine/Threonine Kinase 2) is a kinase that plays a key role in insulin secretion and apoptotic responses. In mice, higher expression of *Brsk2* inhibits insulin secretion through interaction with and phosphorylation of PCTAIRE1, while knockdown of *Brsk2* increases serum insulin levels and produces a tendency towards increased β cell size (28). In our experiments, miR-146a-5p overexpression significantly increased *Brsk2* levels. Another identified target of miR-146a-5p, *Myrip* (Myosin VIIA And Rab Interacting Protein), acts as a scaffolding protein to facilitate exocytosis by promoting immediate fusion of insulin granules with the plasma membrane without predocking (29). Higher expression of *Myrip* in our ZIP cells may represent another mechanism through which miR-146a-5p modulates insulin secretion.

Perp (P53 Apoptosis Effector Related to PMP22), a protein that acts as an effector in the TP53-dependent apoptotic pathway, has been reported as a mediator of β cell dysfunction and apoptosis, and deletion of *Perp* partially preserves β cell function and mass in glucolipotoxicity settings (30). In our study, *Perp*

expression was higher in OE cells than in ZIP cells, and its expression increased significantly under the conditions of cytokine stress, implying a possible mechanism by which miR-146a-5p could mediate β cell apoptosis. *Nrg1* (Neuregulin 1), a member of the epidermal growth factor family, is predicted to be involved in calcium signaling and mitochondrial function. Exposure to recombinant human NRG-1 restores mitochondrial membrane potential, respiration rate, and ATP concentration in cardiomyocytes and skeletal muscle cells in an animal model of heart failure (31). While we observed no change in *Nrg1* expression in OE cells, its upregulation in ZIP cells treated with cytokines suggests that mitochondrial function may be preserved when miR-146a-5p is inhibited.

Together, our results demonstrate a possible new mechanism that defines the significance of miR-146a-5p in the development and progression of T1D.

EXPERIMENTAL PROCEDURES

Isolation and treatment of mouse pancreatic islets

C57/BL6J and female non-obese diabetic (NOD) mice were purchased from Jackson Laboratories and maintained at the Indiana University School of Medicine Laboratory Animal Resource Center under pathogen-free conditions. Protocols were approved by the Indiana University Animal Care and Use Committee. To assess the expression of miR-146a-5p during pro-inflammatory stress, pancreatic islets were isolated from 10-12-week-old C57/BL6J mice as described previously (32). After recovering overnight, islets were hand-picked and treated with a cocktail of pro-inflammatory cytokines: 5 ng/mL IL1β (Cyt-273-b; ProSpec), 100 ng/mL IFNγ (Cyt-358-b; ProSpec), and 10 ng/mL TNFα (Cyt-252-b; ProSpec). Following 24 hours of incubation with cytokines, islets were washed with PBS and stored at -80 °C. To investigate the temporal expression pattern of miR-146a-5p during the progression to T1D, islets were isolated from female NOD mice at 5, 7, 9, 11, and 13 weeks of age, and miR-146a-5p expression was evaluated. For immunofluorescence analysis, pancreatic tissue sections were collected from female NOD mice at 7, 9, 11, and 13 weeks of age. The sections were then assessed for TOM20 and TIM23 expression using immunofluorescence techniques, following previously established protocols (27).

Cell lines

MIN6 cells were grown in DMEM (11965-092; GIBCO) containing 4.5 g/L D-glucose, 4 mM L-glutamine, 10% fetal bovine serum (FBS, 35-015-CV; Corning), 100 units/mL penicillin, 100 µg/mL streptomycin (30-002-CI; Corning), and 50 µM β-mercaptoethanol (034461-100; ThermoFisher Scientific). Cells were cultured at 37 °C in a humidified atmosphere containing 5% CO_2. The medium was changed every other day, and cells were passaged weekly and regularly tested for mycoplasma contamination by PCR-based assay (G238; ABM). To investigate the expression of miR-146a-5p under inflammatory stress, MIN6 cells were cultured in the presence or absence of a combination of three pro-inflammatory cytokines: 5 ng/mL IL1β (Cyt-273; Prospec Protein Specialists), 100 ng/mL IFNγ (Cyt-358; Prospec Protein Specialists), and 10 ng/mL TNFα (Cyt-252; Prospec Protein Specialists) for 24 hours.

Generation of stable miR-146a-5p overexpression or knockdown MIN6 cell lines

MIN6 stable cells with (i) overexpression of miR-146a-5p (OE), (ii) inhibition of miR-146a-5p (ZIP), and (iii) controls with a scrambled sequence bearing no similarity to any known mouse genomic sequence (Scr) were generated using lentiviral vectors. For overexpression of miR-146a-5p, the shMIMIC lentiviral microRNA vector was purchased from Horizon Discovery with Turbo RFP as a reporter (GSH11926-213630770). Lentivector-based scrambled miRZip-000 (MZIP000-PA-1) and miRZip-146a (anti-miRNA; MZIP146a-PA-1) in

S1505A-1 construct vector were purchased from System Biosciences. Both Scrambled and miRZIP vectors contained copGFP as a fluorescent reporter. Upon receipt, glycerol *E. coli* stocks for ZIP and Scr were amplified using an LB broth medium with 100 µg/mL carbenicillin for 24 hours in a bacterial shaker at 37 °C. The bacterial culture was pelleted from LB growth medium for all three vectors, and plasmid DNA was isolated using NucleoSpin® Plasmid (NoLid) kit for miniprep (740499.250; Takara Bio) following manufacturer's instructions. Lentiviruses were generated by transfecting the plasmids using pPACKH1 Packaging Plasmid Mix (LV500A-1; System Biosciences) into a 293T cell line (LV900A-1, 293TN Producer Cell Line; SBI). After 72 hours of culture, viral particles were collected and concentrated using a Lenti-X concentrator (631231; Takara Bio). Lentiviral titers were measured using Lenti-X GoStix (PT5185-2; Clontech, Takara Bio) following instructions provided by the manufacturer. Purified viral particles were transduced into MIN6 cells using TransDux MAX (LV860A-1; System Biosciences) and cultured for 48-72 hours in complete DMEM (11965-092; ThermoFisher Scientific) supplemented with 10% FBS. For clonal selection, transduced cells were cultured with 1 µg/mL puromycin for 7 days. Single clones were picked, seeded in 96-well plates, and cultured with puromycin-containing complete media. The clones were expanded and screened for miR-146a-5p using qRT-PCR, and the clones showing expression patterns of inhibition and overexpression were picked and used for further experiments.

RNA isolation and droplet digital PCR

Total RNA was isolated from mouse islets, MIN6 cells, and organelle fractions using the miRNeasy mini kit (217004; Qiagen) following the manufacturer's instructions. RNA concentration was measured using a NanoDrop 2000 (ThermoFisher Scientific). cDNA was synthesized using the TaqMan MicroRNA Reverse Transcription kit (4366596; ThermoFisher Scientific) according to the manufacturer's instructions.

Droplet digital PCR was used with a few modifications to measure the expression of mmu-miR-146a-5p, as described previously (39). Briefly, 2 µL of cDNA was added to 10 µL of Bio-Rad ddPCR Supermix for Probes (1863024; Bio-Rad), followed by the addition of 1 µL of TaqMan miR-146a-5p 20X primer mix (4427975; Applied Biosystem); final volume was adjusted to 20 µL using RNase- and DNase-free water. Synthetic miR-146a-5p oligo was used as a positive control, and RNase-free water was used as a negative control. The plates were sealed, and droplets were generated using QX200 AutoDG (Bio-Rad) under RNase-free conditions. PCR was performed using a C1000 Thermal Cycler (Bio-Rad), and droplets were read using a QX200 droplet reader (Bio-Rad). Data was analyzed within Quanta Soft™ Software (Bio-Rad). Data are presented as the number of copies/µL.

qRT-PCR for miRNA and mRNA

miScript or miRCURY LNA Primer Assay was used to quantify the expression of miR-146a-5p (MS00003535 or YP00204688; Qiagen) in MIN6 cells or mouse pancreatic islets. One µg of RNA was reverse transcribed using the miRScript II kit (218161; Qiagen) or miRCURY LNA RT Kit (339340; Qiagen). PCR was performed using miScript II (218073; Qiagen) or miRCURY LNA (339371; Qiagen) SYBR Green-based PCR kit. At least three replicates were used per condition. PCR reactions were run in duplicates, and thermal cycling conditions were set according to the manufacturer's instructions. miRScipt II *Rnu*6 (MS00033740; Qiagen) or miRCURY LNA *Rnu6* (YP02119464; Qiagen) was used as the internal reference gene for normalization. Fold-change was calculated using the $2^{-\Delta\Delta}$Ct method (33).

To quantify gene expression, 500 ng of total RNA was reverse transcribed using the M-MLV RT kit (28025013; Invitrogen). TaqMan Fast Advanced Master Mix (4444557; ThermoFisher Scientific) and gene-specific probes for *Mapt* (Mm00521988_m1), *Myrip* (Mm00460563_m1),

Brsk2 (Mm01279141_m1), *Glrx* (Mm00728386_s1), *Acvr2b* (Mm00431664_m1), *Rest* (Mm00803268_m1), *Perp* (Mm00480750_m1), *Eya1* (Mm00438796_m1), *Sort1* (Mm00490905_m1), *Gpx1* (Mm00656767_g1) and *Nrg1* (Mm01212130_m1) were used. Thermal cycling conditions specified for the Taqman Fast Advanced master mix were followed. *Actb* (Mm02619580_g1) was used as the internal reference gene for normalization. PCR reactions were run in duplicates, and four replicates per condition were used. Fold-change was calculated using the $2^{-\Delta\Delta}$Ct method (33).

Cell death assessment

Cell death assessment was performed using the Sartorius IncuCyte S3 live-cell analysis equipment (Sartorius, Göttingen, Germany) housed at the Indiana University School of Medicine. Briefly, WT MIN6 cells with no viral vector, and Scr, ZIP, and OE MIN6 cells were plated on 96-well cell culture plates and analyzed starting at ~40-50% confluency. Cells were transferred to the scanning instrument, and cell media containing dyes for detection of exposed phosphatidylserine, a marker for apoptosis, was added to the cells. Annexin-V green was added to WT and OE cells, and Annexin-V Red was added to WT, Scr, and ZIP cells (1:1000 dilution, #4642 and #4641, Sartorius, Ann Arbor, MI - USA) immediately before time 0 of IncuCyte scan. Cytokines were added or not to the media of each cell line immediately before the first scan. Five images from different areas of each well were collected with a 10X objective every hour for 48 hours, and cell death was quantified as the average number of green or red fluorescent counted objects (excitation: 488nm; emission: 523nm) per unit area at each time point and normalized by percent confluency in each scanned area. Cell death over 48 hours was expressed relative to cell death at time 0 within each replicate.

mRNA sequencing and data analysis

Total RNA was assessed for quality based on RNA integrity number (RIN) using an Agilent Bioanalyzer 2100. All samples had good-quality RNA, with RIN ranging from 9.6 to 9.9. One hundred nanograms of total RNA was used for library preparation. Briefly, cDNA library preparation included mRNA purification, RNA fragmentation, cDNA synthesis, and ligation of index adaptors. Library amplification was performed following the KAPA mRNA Hyper Prep Kit Technical Data Sheet (KR1352 – v4.17, Roche Corporate). Each resulting indexed library was quantified, and its quality was assessed by Qubit and Agilent Bioanalyzer, and multiple libraries were pooled in equal molarity. The pooled libraries were sequenced with a 2×100 bp paired-end configuration on the Illumina NovaSeq 6000 sequencer using the v1.5 Reagent Kit. Approximately 30M reads per library were generated. A Phred quality score (Q score) was used to measure the quality of sequencing. More than 90% of the sequencing reads reached Q30 (99.9% base call accuracy).

The quality of sequencing data was first assessed using FastQC (Babraham Bioinformatics). Further analysis using Fastq files was performed using Partek Flow 10.0.21.0718. Sequencing files were aligned to the mm10 mouse reference genome using STAR aligner 2.7.3a and mapped to mRNA using RefSeq Transcripts 96 annotation database. Genes with less than 10 read counts in total were removed. Differential expression analysis was performed using DESeq2, and genes with fold-change ≥ 1.5 and p-value < 0.05 were considered as differentially expressed. All comparisons were made using Scr as the control group. Raw data along with raw counts and normalized values (median ratio values) are deposited in NCBI GEO under the accession ID GSE255756.

Functional enrichment and identification of mRNA targets

The DAVID bioinformatics tool was used for functional enrichment analysis (34, 35). Differentially expressed genes from each comparison pair were provided as input for gene ontology analysis. For each comparison, gene ontology terms with fold enrichment value ≥ 1.5 and p-value < 0.05 were retained for further analysis. Since the objective of the study was to

identify the role of miR-146a-5p in T1D pathogenesis, we focused on gene ontology terms containing the following keywords: mitochondria, endoplasmic reticulum, Golgi, insulin, glucose, apoptosis, cell death, reactive oxygen species, oxidative stress, ATP, zinc, calcium, exocytosis, phagocytosis, and antigen processing and presentation.

To identify the molecular targets that are predicted to bind with the seed sequence of miR-146a-5p, first, *in silico* target prediction was performed with TargetScan 7.2 using a mouse genome as the input (36). We used all the targets, irrespective of the target site conservation status. Targets identified from TargetScan were overlapped with genes included in functional terms containing "cell death," "apoptosis," "insulin," and "mitochondria." These hits were further filtered to the differentially expressed genes generated from ZIP vs. Scr and OE vs. Scr comparisons. Specifically, we only included genes that showed opposite directions of expression between the two comparison pairs. Ten representative targets were selected for validation using qRT-PCR. Although *Gpx1* was not predicted to be a direct target, we included it because of its role in oxidative stress and its opposing expression pattern in ZIP and OE cells.

Isolation of mitochondria and cytoplasm

Mitochondria and cytoplasm from MIN6 cells were isolated using methods described previously (37). Briefly, $2x10^6$ cells were seeded in a 10 cm culture dish and cultured for 3 days. After 3 days, the cells were replenished with fresh culture media and treated with or without IL1β + IFNγ + TNFα for 24 hours. After the treatment period, the cells were trypsinized with 0.05% trypsin, resuspended with 1X PBS (14190-144; Gibco), and transferred to a 15 mL tube. The cells were pelleted at 215 x g for 5 minutes at 4 °C. The supernatant was discarded, and the cells were resuspended in 500 µL of hypotonic buffer (50 mM HEPES, 1 mM EDTA (pH 8.0), 1 mM Dithiothreitol (DTT), 1X protease inhibitor cocktail (635673; Takara Clontech), 1 mM PMSF, and 1 mg/mL BSA Fraction V) and incubated on ice for 5 minutes. The cells were lysed using digitonin at a final concentration of 0.02% and vortexed every 10 seconds for 5 minutes and mixed with 1:1 (v/v) of 2X isotonic buffer (100 mM HEPES, 2 mM EDTA (pH 8.0), 2 mM DTT, 1X Protease inhibitor cocktail, 2 mM PMSF, 2 mg/mL BSA, and 1.2 M D-Sorbitol) and centrifuged at 700 x g for 10 minutes at 4 ºC. After centrifugation, the supernatant was transferred to a new 1.5 mL tube and centrifuged at 10,000 x g for 15 minutes at 4 ºC. Again, the supernatant was transferred to a new 1.5 mL tube (cytoplasmic fraction) and stored at -80 ºC. 1X isotonic buffer was added on top of the mitochondria pellet and centrifuged at 10,000 x g for 5 minutes at 4 ºC. The supernatant was removed and the pellet containing mitochondria was stored at -80 ºC until further use. To identify the expression of miR-146 in mitochondria, total mitochondrial-enriched or cytoplasm-enriched miRNAs were isolated using the Qiagen miRNeasy kit as described above.

Mitochondrial metabolic assay

MIN6 stable cell lines were subjected to the Seahorse XF Cell Mito Stress test (103015-100; Agilent). The cells were seeded in the Seahorse XFe 96-well plate at 5,000 cells/well and cultured for 24 hours. The medium was changed the following day, and the cells were treated with pro-inflammatory cytokines for an additional 24 hours. Forty-eight hours post seeding, the growth medium was exchanged for glucose-free, Seahorse Phenol red-free DMEM with 200 mM glutamine, and 100 mM pyruvate, and incubated for 1 hour at 37 °C. Subsequently, cells were incubated for 1 hour with a DMEM containing 2.5 mM glucose in a non-CO_2 incubator at 37 °C. Oxygen consumption rate (OCR) was measured in 2.5 mM glucose- DMEM as the baseline measurement and following 25 mM glucose stimulus, and mitochondrial inhibitors oligomycin, carbonyl cyanide-4-(trifluoromethoxy) phenylhydrazone (FCCP) and rotenone/antimycin A, respectively, according to the manufacturer's instructions. Cell count/well was calculated using 10X phase contrast images with segmentation (Incucyte). Counts per image were extrapolated to total counts per well using the surface area of each well (10.326 mm^2) and image area (2.275 mm^2), i.e., a multiplication factor of 4.538901. The following assay parameters were assessed in the Mito Stress test:

basal respiration, maximal respiration, non-mitochondrial respiration, proton leak, ATP production, and spare respiratory capacity. All reactions were run using six replicates per condition, and the assay was repeated five times. OCR data were normalized using the number of cells/well.

Assessment of mitochondrial DNA copy number

Scr, ZIP, and OE MIN6 cells were cultured in the presence or absence of pro-inflammatory cytokines for 24 hours. Genomic DNA was extracted using a Qiagen DNeasy kit (69504; Qiagen) according to the manufacturer's instructions and quantified using a Nanodrop spectrophotometer. Ten nanograms of genomic DNA was added to each qPCR reaction (5 µL of BioRad SYBR green 2X master Mix, 0.4 µL of 10 µM forward primer, 0.4µL of 10 µM reverse primer, 2.2 µL of nuclease-free water, and 2 µL of cDNA at 5 ng/µL). Samples were heated to 98 °C for 5 min, then cycled 40 times at 98 °C for 15 sec followed by 60 °C for 30 sec. Samples were then heated to 95 °C, cooled to 60 °C for 1 min, and then re-heated to 95 °C for melting curve analysis. At least three replicates were used, and the samples were run in technical duplicates. Mitochondria-specific DNA *Nd1* was used for estimating the copy number, and the reference genes were nuclear DNA-specific *Tbp* and *Hprt*.

Mitochondrial DNA copy number was calculated using the formula: $\Delta Ct = Ct(nDNA\ gene) - Ct(mtDNA\ gene)$. Copies of mtDNA = $2 \times 2^{\Delta Ct}$. Primer sequences for mitochondria-encoded and nuclear-encoded genes are provided in Table S3.

Electron microscopy imaging

MIN6 Scr, ZIP, and OE stable cells were seeded in a 6-well plate with a density of $2x10^6$ cells/well and cultured in complete DMEM for 48 hours and were treated with pro-inflammatory cytokines (IL1β, IFNγ and TNFα) for 24 hours. MIN6 stable cells not treated with cytokines were considered as control cells. The cells were washed twice with plain DMEM and fixed with 2.5% glutaraldehyde and 4% paraformaldehyde in 0.1 mol/L sodium cacodylate buffer. The cells were collected by scraping the wells, transferred to a 1.5 mL centrifuge tube, and shipped to the Advanced Electron Microscopy Facility at the University of Chicago for electron microscope analysis. Images were analyzed using ImageJ (38) to estimate the number and assess the overall morphology of the mitochondria.

Immunofluorescence staining

Formalin-fixed paraffin-embedded (FFPE) pancreatic tissues from NOD mice were sectioned with 5 µm thickness and dewaxed at 70 °C according to the methods described previously (27). Briefly, the slides were deparaffinized with xylene twice for 7 minutes and hydrated with a series of different concentrations of alcohol. Antigen retrieval was performed using citrate buffer (H-3300; Vector Laboratories Inc) for 15 minutes at 100 °C, and the slides in the buffer were cooled to room temperature for 20 minutes and washed with 1X PBS twice for 5 minutes. The slides were blocked with animal free blocker (SP-5030; Vector Laboratories Inc) for 1 hour and incubated with primary antibodies against TOM20 (1:200; 42406S; Cell Signaling), TIM23 (1:200; BD-611222; BD Biosciences), or insulin (IR002; Dako) overnight at 4 °C. Then the slides were washed twice with 1X PBS for 5 minutes and incubated with secondary antibodies: Alexa-Fluor 488 goat anti-guinea pig (A11073; Invitrogen), Alexa-Fluor 568 goat anti-mouse (A11031; Invitrogen), and Alexa-Fluor 647 donkey anti-rabbit (A31573; Invitrogen), and counterstained with DAPI for nucleus.

For immunostaining of MIN6 cells, 75,000 cells were seeded per well in an 8-well chamber slide (80841; Ibidi) and incubated for 24 hours. The following day, cells were treated with or without pro-inflammatory cytokines for another 24 hours. Cells were washed twice with 1X PBS and fixed with 4% paraformaldehyde for 30 minutes at 37 °C. After permeabilizing with 0.1% Triton X-100 in PBS (twice for 5 minutes), the cells were blocked using 0.1% FBS in PBS for 1 hour. The cells were then incubated overnight at 4 °C with primary antibody against TIM23 (1:200; BD-611222; BD Biosciences) diluted in PBS supplemented with 5% FBS. The cells were washed three times with 0.1% Triton X-100 in PBS (5 minutes each wash) and

incubated with a secondary goat anti-mouse antibody (Alexa 647; 1:200) for 2 hours at room temperature. After washing the cells three times with 0.1% Triton X-100 in PBS, nuclei were stained with DAPI for 15 minutes at room temperature. Cells were washed twice with 0.1% Triton X-100 in PBS and mounted with Fluorsave reagent (345789-20ML; Millipore Sigma). Z-stack images were acquired using an LSM 800 confocal microscope (Carl Zeiss, Germany). Fluorescence intensity was measured using Image J software (NIH).

Western blotting

Scr, ZIP, and OE MIN6 cells were cultured in a 12-well plate at a seeding density of $4x10^5$ cells/well. Once the cells reached ~75-80% confluency, they were treated with pro-inflammatory cytokines for 24 hours. After treatment, the cells were washed with PBS and lysed with lysis buffer (50 mM Tris-HCL, 150 mM NaCl, 0.05% Deoxycholate, 0.1% IGEPAL, 0.1% SDS, 0.2% x Sarcosyl, 5% Glycerol, 1mM DTT, 1 mM EDTA, 2 mM $MgCL_2$, Protease inhibitor (04693132001; Roche, Complete mini-EDTA free), and phosphatase inhibitor (04906837001; Roche, PhosphoStop). Protein concentrations were determined using Lowry's method. Twenty micrograms of protein per sample was heated for 10 minutes at 70 °C and immediately placed on ice. Proteins were separated using a 4-12% Bis-Tris plus gel (NW04122BOX; Invitrogen) and transferred to a PVDF membrane. Membranes were blocked with Intercept blocking buffer (927-70001; LI-COR) and incubated overnight at 4 °C with primary antibodies against β-tubulin (2128; Cell Signaling), caspase-3 (9662; Cell Signaling), and cleaved caspase-3 (9664; Cell Signaling). Membranes were then washed with 0.05% phosphate buffered saline-Tween (PBS-T) for 20 minutes and incubated with donkey anti-rabbit and donkey anti-goat secondary antibodies (LI-COR) for 2 hours. Images were acquired using an LI-COR image scanner, and protein was quantified using ImageStudio software.

Statistical analysis.

All statistical analyses (except for the analysis of RNA sequencing data) were performed using GraphPad Prism version 9.2. For comparison of means between the two groups, a two-tailed unpaired Student's *t*-test was used. One-way ANOVA was used for the comparison of means among three or more groups. In all tests, $p < 0.05$ was considered to be statistically significant. Data are presented as mean ± standard error of the mean (SEM). Graphs were generated using GraphPad Prism.

Author Contributions:

P.K, F.S, and C.E.M conceived the study and designed the experiments; P.K, F.S, S.A.W, R.C.S.B, G.C, and C.L performed experiments and analyzed and interpreted the data; C.E.M supervised the study and acquired funds to conduct the study; P.K wrote the draft of the manuscript. All authors reviewed and edited the manuscript.

Funding and Acknowledgements:

This work was supported by NIH grants R01 DK093954, DK127308, U01DK127786, and UC4 DK104166 (to CEM), VA Merit Award I01BX001733 (to CEM), 2-SRA-2019-834-S-B, JDRF 2-SRA-2018-493-A-B, and 3-IND-2022-1235-I-X (to CEM), and gifts from the Sigma Beta Sorority, the Ball Brothers Foundation, and the George and Frances Ball Foundation (to CEM). FS was supported by JDRF awards (3-PDF-20016-199-A-N and JDRF 5-CDA-2022-1176-A-N) and by NIH/NIDDK dkNET (U24DK097771). SAW was supported by an F31 Fellowship from the National Institute of Diabetes and Digestive and Kidney Diseases (NIDDK) award F31DK134168 and a TL1 fellowship from the National Center for Advancing Translational Sciences, Clinical and Translational Sciences Award UL1TR002529. The authors acknowledge the support of the Islet and Physiology Core and the Translation Core of the Indiana Diabetes Research Center (2P30DK097512). The authors also thank Kara Orr and Lata Udari from Islet and Physiology Core for their assistance with islet isolation. We thank Dr. Emily Anderson-Baucum for her suggestions and assistance in editing the text of this manuscript.

Conflicts of Interest

Dr. Evans-Molina reports serving on advisory boards related to T1D research clinical trial initiatives: Provention Bio, Dompe Pharmaceuticals, Isla Technologies, MaiCell Technologies, Avotres, DiogenX and Neurodon. CEM serves as President of the Immunology of Diabetes Society (IDS), Co-Executive Director of the Network for Pancreatic Organ Donors with Diabetes (nPOD), Co-PI of the NIH Integrated Islet Distribution Program (IIDP), and a member of the Type 1 Diabetes Clinical Network. CEM serves on the external advisory board for INNODIA receiving in-kind research support from Bristol Myers Squibb and Nimbus Pharmaceuticals; receiving investigator-initiated grants from Lilly Pharmaceuticals and Astellas Pharmaceuticals. CEM has patent (16/291,668) Extracellular Vesicle Ribonucleic Acid (RNA) Cargo as a Biomarker of Hyperglycaemia and Type 1 Diabetes and provisional patent (63/285,765) Biomarker for Type 1 Diabetes (PDIA1 as a biomarker of β cell stress).

REFERENCES

1. DiMeglio, L. A., Evans-Molina, C., and Oram, R. A. (2018) Type 1 diabetes. *Lancet*. **391**, 2449–2462
2. Lebastchi, J., and Herold, K. C. (2012) Immunologic and Metabolic Biomarkers of β-Cell Destruction in the Diagnosis of Type 1 Diabetes. *Cold Spring Harb Perspect Med*. **2**, a007708
3. Ziegler, A. G., Rewers, M., Simell, O., Simell, T., Lempainen, J., Steck, A., Winkler, C., Ilonen, J., Veijola, R., Knip, M., Bonifacio, E., and Eisenbarth, G. S. (2013) Seroconversion to multiple islet autoantibodies and risk of progression to diabetes in children. *JAMA*. **309**, 2473–2479
4. Eizirik, D. L., Sammeth, M., Bouckenooghe, T., Bottu, G., Sisino, G., Igoillo-Esteve, M., Ortis, F., Santin, I., Colli, M. L., Barthson, J., Bouwens, L., Hughes, L., Gregory, L., Lunter, G., Marselli, L., Marchetti, P., McCarthy, M. I., and Cnop, M. (2012) The human pancreatic islet transcriptome: expression of candidate genes for type 1 diabetes and the impact of pro-inflammatory cytokines. *PLoS Genet*. **8**, e1002552
5. Wu, W., Syed, F., Simpson, E., Lee, C.-C., Liu, J., Chang, G., Dong, C., Seitz, C., Eizirik, D. L., Mirmira, R. G., Liu, Y., and Evans-Molina, C. (2021) The Impact of Pro-Inflammatory Cytokines on Alternative Splicing Patterns in Human Islets. *Diabetes*. 10.2337/db20-0847
6. Krishnan, P., Syed, F., Jiyun Kang, N., Mirmira, R. G., and Evans-Molina, C. (2019) Profiling of RNAs from Human Islet-Derived Exosomes in a Model of Type 1 Diabetes. *Int J Mol Sci*. **20**, 5903
7. Syed, F., Krishnan, P., Chang, G., Langlais, S. R., Hati, S., Yamada, K., Lam, A. K., Talware, S., Liu, X., Sardar, R., Liu, J., Mirmira, R. G., and Evans-Molina, C. (2023) β Cell microRNAs Function as Molecular Hubs of Type 1 Diabetes Pathogenesis and as Biomarkers of Diabetes Risk. *bioRxiv*. 10.1101/2023.06.15.545170
8. Lakhter, A. J., Pratt, R. E., Moore, R. E., Doucette, K. K., Maier, B. F., DiMeglio, L. A., and Sims, E. K. (2018) Beta cell extracellular vesicle miR-21-5p cargo is increased in response to inflammatory cytokines and serves as a biomarker of type 1 diabetes. *Diabetologia*. **61**, 1124–1134
9. Bartel, D. P. (2004) MicroRNAs: genomics, biogenesis, mechanism, and function. *Cell*. **116**, 281–297
10. Lee, R. C., Feinbaum, R. L., and Ambros, V. (1993) The C. elegans heterochronic gene lin-4 encodes small RNAs with antisense complementarity to lin-14. *Cell*. **75**, 843–854
11. Wightman, B., Ha, I., and Ruvkun, G. (1993) Posttranscriptional regulation of the heterochronic gene lin-14 by lin-4 mediates temporal pattern formation in C. elegans. *Cell*. **75**, 855–862
12. Kredo-Russo, S., Mandelbaum, A. D., Ness, A., Alon, I., Lennox, K. A., Behlke, M. A., and Hornstein, E. (2012) Pancreas-enriched miRNA refines endocrine cell differentiation. *Development*. **139**, 3021–3031
13. Latreille, M., Herrmanns, K., Renwick, N., Tuschl, T., Malecki, M. T., McCarthy, M. I., Owen, K. R., Rülicke, T., and Stoffel, M. (2015) miR-375 gene dosage in pancreatic β-cells: implications for regulation of β-cell mass and biomarker development. *J Mol Med (Berl)*. **93**, 1159–1169
14. Poy, M. N., Eliasson, L., Krutzfeldt, J., Kuwajima, S., Ma, X., Macdonald, P. E., Pfeffer, S., Tuschl, T., Rajewsky, N., Rorsman, P., and Stoffel, M. (2004) A pancreatic islet-specific microRNA regulates insulin secretion. *Nature*. **432**, 226–230
15. Poy, M. N., Hausser, J., Trajkovski, M., Braun, M., Collins, S., Rorsman, P., Zavolan, M., and Stoffel, M. (2009) miR-375 maintains normal pancreatic alpha- and beta-cell mass. *Proc Natl Acad Sci U S A*. **106**, 5813–5818
16. Sims, E. K., Lakhter, A. J., Anderson-Baucum, E., Kono, T., Tong, X., and Evans-Molina, C. (2017) MicroRNA 21 targets BCL2 mRNA to increase apoptosis in rat and human beta cells. *Diabetologia*. **60**, 1057–1065
17. Roggli, E., Britan, A., Gattesco, S., Lin-Marq, N., Abderrahmani, A., Meda, P., and Regazzi, R. (2010) Involvement of microRNAs in the cytotoxic effects exerted by proinflammatory cytokines on pancreatic beta-cells. *Diabetes*. **59**, 978–986
18. Dasgupta, N., Peng, Y., Tan, Z., Ciraolo, G., Wang, D., and Li, R. (2015) miRNAs in mtDNA-less cell mitochondria. *Cell Death Discov*. **1**, 15004

19. Li, P., Jiao, J., Gao, G., and Prabhakar, B. S. (2012) Control of mitochondrial activity by miRNAs. *J Cell Biochem*. **113**, 1104–1110
20. Bian, Z., Li, L.-M., Tang, R., Hou, D.-X., Chen, X., Zhang, C.-Y., and Zen, K. (2010) Identification of mouse liver mitochondria-associated miRNAs and their potential biological functions. *Cell Res*. **20**, 1076–1078
21. Haythorne, E., Rohm, M., van de Bunt, M., Brereton, M. F., Tarasov, A. I., Blacker, T. S., Sachse, G., Silva Dos Santos, M., Terron Exposito, R., Davis, S., Baba, O., Fischer, R., Duchen, M. R., Rorsman, P., MacRae, J. I., and Ashcroft, F. M. (2019) Diabetes causes marked inhibition of mitochondrial metabolism in pancreatic β-cells. *Nat Commun*. **10**, 2474
22. Kwak, S. H., Park, K. S., Lee, K.-U., and Lee, H. K. (2010) Mitochondrial metabolism and diabetes. *J Diabetes Investig*. **1**, 161–169
23. Szabadkai, G., and Duchen, M. R. (2009) Mitochondria mediated cell death in diabetes. *Apoptosis*. **14**, 1405–1423
24. Fazzini, F., Lamina, C., Raftopoulou, A., Koller, A., Fuchsberger, C., Pattaro, C., Del Greco, F. M., Döttelmayer, P., Fendt, L., Fritz, J., Meiselbach, H., Schönherr, S., Forer, L., Weissensteiner, H., Pramstaller, P. P., Eckardt, K.-U., Hicks, A. A., Kronenberg, F., and GCKD Investigators (2021) Association of mitochondrial DNA copy number with metabolic syndrome and type 2 diabetes in 14 176 individuals. *J Intern Med*. **290**, 190–202
25. Petersen, K. F., Dufour, S., Befroy, D., Garcia, R., and Shulman, G. I. (2004) Impaired mitochondrial activity in the insulin-resistant offspring of patients with type 2 diabetes. *N Engl J Med*. **350**, 664–671
26. Picard, M., Shirihai, O. S., Gentil, B. J., and Burelle, Y. (2013) Mitochondrial morphology transitions and functions: implications for retrograde signaling? *American Journal of Physiology-Regulatory, Integrative and Comparative Physiology*. 10.1152/ajpregu.00584.2012
27. Syed, F., Singhal, D., Raedschelders, K., Krishnan, P., Bone, R. N., McLaughlin, M. R., Van Eyk, J. E., Mirmira, R. G., Yang, M.-L., Mamula, M. J., Wu, H., Liu, X., and Evans-Molina, C. (2023) A discovery-based proteomics approach identifies protein disulphide isomerase (PDIA1) as a biomarker of β cell stress in type 1 diabetes. *EBioMedicine*. **87**, 104379
28. Chen, X.-Y., Gu, X.-T., Saiyin, H., Wan, B., Zhang, Y.-J., Li, J., Wang, Y.-L., Gao, R., Wang, Y.-F., Dong, W.-P., Najjar, S. M., Zhang, C.-Y., Ding, H.-F., Liu, J. O., and Yu, L. (2012) Brain-selective kinase 2 (BRSK2) phosphorylation on PCTAIRE1 negatively regulates glucose-stimulated insulin secretion in pancreatic β-cells. *J Biol Chem*. **287**, 30368–30375
29. Wang, H., Mizuno, K., Takahashi, N., Kobayashi, E., Shirakawa, J., Terauchi, Y., Kasai, H., Okunishi, K., and Izumi, T. (2020) Melanophilin Accelerates Insulin Granule Fusion without Predocking to the Plasma Membrane. *Diabetes*. **69**, 2655–2666
30. Huang, Q., You, W., Li, Y., Sun, Y., Zhou, Y., Zhang, Y., Liu, D., Zhan, S., Zhu, Y., and Han, X. (2018) Glucolipotoxicity-Inhibited miR-299-5p Regulates Pancreatic β-Cell Function and Survival. *Diabetes*. **67**, 2280–2292
31. Guo, Y., Zhang, X., Liu, Y., Duan, H., Jie, B., and Wu, X. (2012) Neuregulin-1 attenuates mitochondrial dysfunction in a rat model of heart failure. *Chin Med J (Engl)*. **125**, 807–814
32. Stull, N. D., Breite, A., McCarthy, R., Tersey, S. A., and Mirmira, R. G. (2012) Mouse islet of Langerhans isolation using a combination of purified collagenase and neutral protease. *J Vis Exp*. 10.3791/4137
33. Livak, K. J., and Schmittgen, T. D. (2001) Analysis of relative gene expression data using real-time quantitative PCR and the 2(-Delta Delta C(T)) Method. *Methods*. **25**, 402–408
34. Sherman, B. T., Hao, M., Qiu, J., Jiao, X., Baseler, M. W., Lane, H. C., Imamichi, T., and Chang, W. (2022) DAVID: a web server for functional enrichment analysis and functional annotation of gene lists (2021 update). *Nucleic Acids Res*. **50**, W216–W221
35. Huang, D. W., Sherman, B. T., and Lempicki, R. A. (2009) Systematic and integrative analysis of large gene lists using DAVID bioinformatics resources. *Nat Protoc*. **4**, 44–57

36. Agarwal, V., Bell, G. W., Nam, J.-W., and Bartel, D. P. (2015) Predicting effective microRNA target sites in mammalian mRNAs. *eLife*. **4**, e05005
37. Dixit, B., Vanhoozer, S., Anti, N. A., O'Connor, M. S., and Boominathan, A. (2021) Rapid enrichment of mitochondria from mammalian cell cultures using digitonin. *MethodsX*. **8**, 101197
38. Lam, J., Katti, P., Biete, M., Mungai, M., AshShareef, S., Neikirk, K., Garza Lopez, E., Vue, Z., Christensen, T. A., Beasley, H. K., Rodman, T. A., Murray, S. A., Salisbury, J. L., Glancy, B., Shao, J., Pereira, R. O., Abel, E. D., and Hinton, A. (2021) A Universal Approach to Analyzing Transmission Electron Microscopy with ImageJ. *Cells*. **10**, 2177

Figure Legends:

Figure 1. Pro-inflammatory stress increases miR-146a-5p expression levels, leading to increased cell death of MIN6 cells. (A) ddPCR results to determine the expression of miR-146a-5p in mouse islets (n=8). (B) qRT-PCR results to determine miR-146a-5p expression levels in MIN6 cells treated with/without pro-inflammatory cytokines (n=6). (C) qRT-PCR results to determine expression levels of miR-146a-5p in untreated MIN6 stable cells expressing scrambled sequence (Scr), inhibition (ZIP), and overexpression (OE) of miR-146a-5p (n=2). (D-F) Cell death assessment assay (n=5) using Incucyte comparing WT and Scr groups (D), WT and ZIP groups (E), and WT and OE groups (F). Data is presented as means ± SEM. For all comparisons, *p*-values are indicated above.

Figure 2. RNA sequencing from MIN6 stable cells show modulation of mitochondrial pathways. (A) PCA plot including all six (Scr, ZIP, OE, Scr+Cy, ZIP+Cy and OE+Cy) comparison groups (n=3-4). (B) Number of differentially expressed genes from each comparison. The comparison groups are indicated below each bar. Red indicates upregulated genes and blue indicates downregulated genes. The numbers included within each bar indicate the number of up and downregulated genes. (C) Functional enrichment results including all comparison groups. Each column represents one group compared to the scrambled (Scr) group. Numbers within each box indicate the fold enrichment value. Higher values are represented by purple and lower values are represented by yellow. Boxes without any numbers indicate no enrichment of the function for that comparison.

Figure 3. Pro-inflammatory stress increases miR-146a-5p expression levels in mitochondria and cytoplasm and inhibition of miR-146a-5p increases respiratory capacity of MIN6 cells. (A-B) ddPCR to determine the expression of miR-146a-5p in cytoplasm (A) and mitochondria (B) in the presence and absence of pro-inflammatory cytokines (n=2). (C) Normalized oxygen consumption rate calculated over time (minutes) in stable MIN6 cells in the presence and absence of pro-inflammatory cytokines. (D-I) Assessment of other parameters of mitochondrial function including basal respiration (D), maximal respiration (E), spare respiratory capacity (F), proton leak (G), ATP production (H), and non-mitochondrial oxygen consumption (I) (n=5). Data is presented as means ± SEM.

Figure 4. Inhibition of miR-146a-5p increases mitochondrial copy number and mitochondria content in MIN6 cells. (A) Mitochondria DNA copy number in MIN6 stable cells (n=3) is presented as the ratio of mitochondrial DNA (*Nd1*) to the geometric mean of two nuclear encoded genes (*Tbp, Hprt*). (B) Electron microscopy images of MIN6 stable cells in the presence and absence of pro-inflammatory cytokines (n=1). M = mitochondria, IG = Insulin granule, N = nucleus, G = Golgi, ER = Endoplasmic reticulum. Scale bar = 500 nm.

Figure 5. miR-146a-5p overexpression decreases TIM23 expression levels in MIN6 cells. Immunostaining and quantification of TIM23 expression in MIN6 stable cells (n=3). All groups were compared to Scr. Data is presented as means ± SEM.

Figure 6. Validation of miR-146a-5p targets. qRT-PCR results of ten predicted targets of miR-146a-5p in MIN6 stable cells (n=4). Data is presented as means ± SEM.

Figure 7. Time-dependent decrease in TOM20 and TIM23 and increase in miR-146a-5p expression in pancreatic islets from NOD mice. (A) Immunostaining of TOM20, TIM23, INS, and DAPI in pancreatic tissue sections of 7-, 9-, 11- and 13-week-old NOD mice (n=8). (B) Quantification of TOM20 and (C) TIM23 using ImageJ. (D) qRT-PCR results to determine time-dependent expression of miR-146a-5p levels in islets isolated from 5-, 7-, 9-, 11- and 13-week old NOD mice (n=8).

Supplementary Figure Legends

Figure S1. Pro-inflammatory stress increased miR-146a-5p expression in MIN6 stable cells. (A-C) Fold change values from qRT-PCR experiments (n=6) to determine expression levels of miR-146a-5p in Scr and Scr+Cy MIN6 cells (A), ZIP and ZIP+Cy MIN6 cells (B), and OE and OE+Cy MIN6 cells (C). (D-F) Incucyte live cell image system to track cell death (represented by green or red fluorescence) over time. Cell death was compared between WT and Scr (D), WT and ZIP (E), and WT and OE (F). Scale = 400 µm.

Figure S2. Overexpression of miR-146a-5p increases cleaved caspase-3 levels under pro-inflammatory stress. (A) Western blot image showing abundance of caspase-3 and cleaved caspase-3 proteins in MIN6 cells (n=4) treated with/without pro-inflammatory cytokines. (B) Quantification of western blots. Data is presented as means + SEM and statistical significance is determined by one way ANOVA.

Figure S3. Assessment of mitochondrial architecture in cytokine-treated and untreated MIN6 stable cell lines. (A-F) Comparison of number of mitochondria (A), mitochondria perimeter (B), Feret diameter (C), mitochondria aspect ratio (D), mitochondria circularity (E), and mitochondria roundness (F) across all groups (n=1).

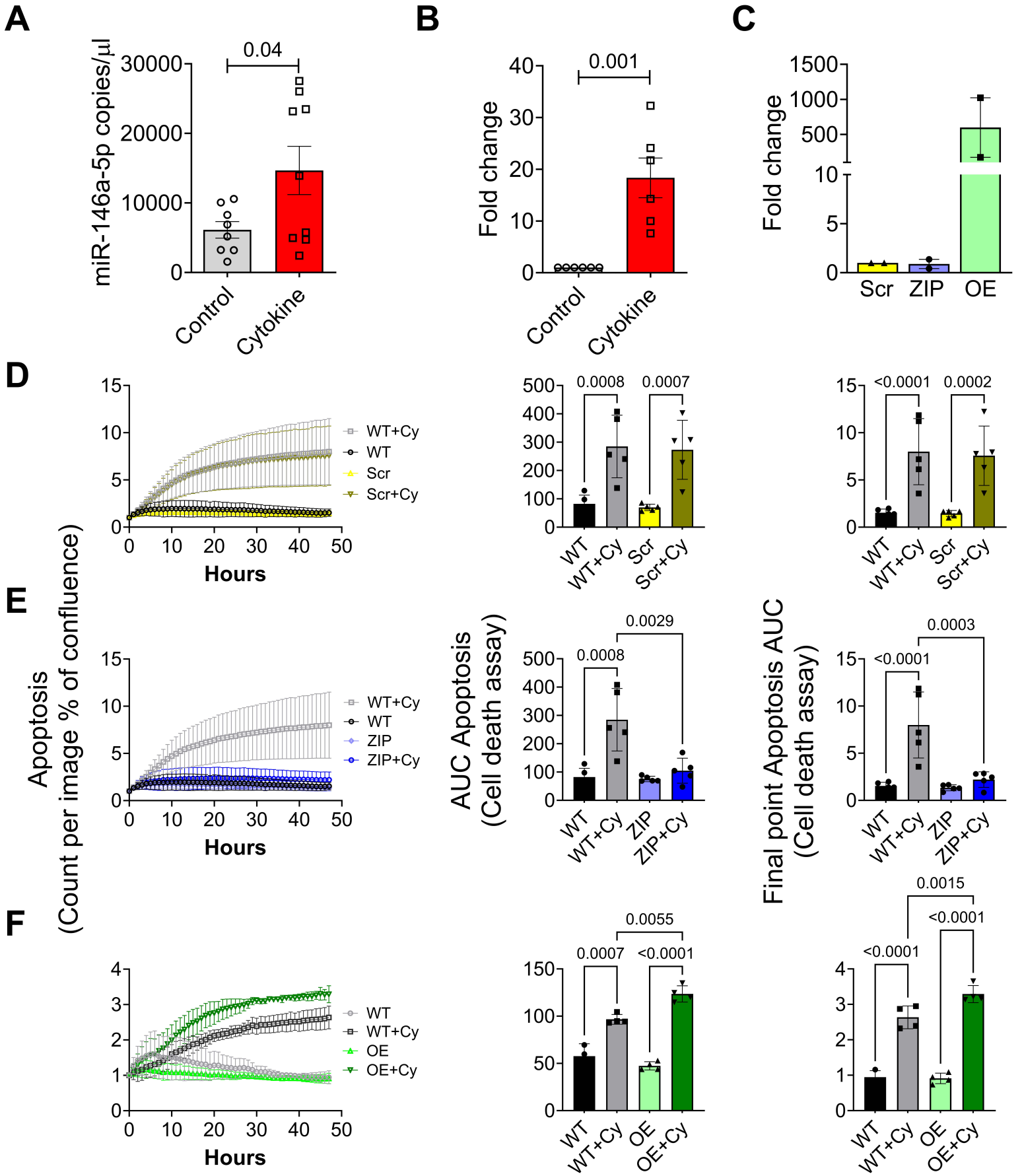
A
miR-146a-5p copies/µl
30000
20000
10000
0
0.04
Control
Cytokine
B
Fold change
40
30
20
10
0
0.001
Control
Cytokine
C
Fold change
1500
1000
500
10
5
0
Scr
ZIP
OE
D
Apoptosis
(Count per image % of confluence)
15
10
5
0
0
10
20
30
40
50
Hours
WT+Cy
WT
Scr
Scr+Cy
500
400
300
200
100
0
0.0008
0.0007
WT
WT+Cy
Scr
Scr+Cy
15
10
5
0
<0.0001
0.0002
WT
WT+Cy
Scr
Scr+Cy
E
15
10
5
0
0
10
20
30
40
50
Hours
WT+Cy
WT
ZIP
ZIP+Cy
AUC Apoptosis
(Cell death assay)
500
400
300
200
100
0
0.0029
0.0008
WT
WT+Cy
ZIP
ZIP+Cy
Final point Apoptosis AUC
(Cell death assay)
15
10
5
0
0.0003
<0.0001
WT
WT+Cy
ZIP
ZIP+Cy
F
4
3
2
1
0
0
10
20
30
40
50
Hours
WT
WT+Cy
OE
OE+Cy
150
100
50
0
0.0055
0.0007
<0.0001
WT
WT+Cy
OE
OE+Cy
4
3
2
1
0
0.0015
<0.0001
<0.0001
WT
WT+Cy
OE
OE+Cy

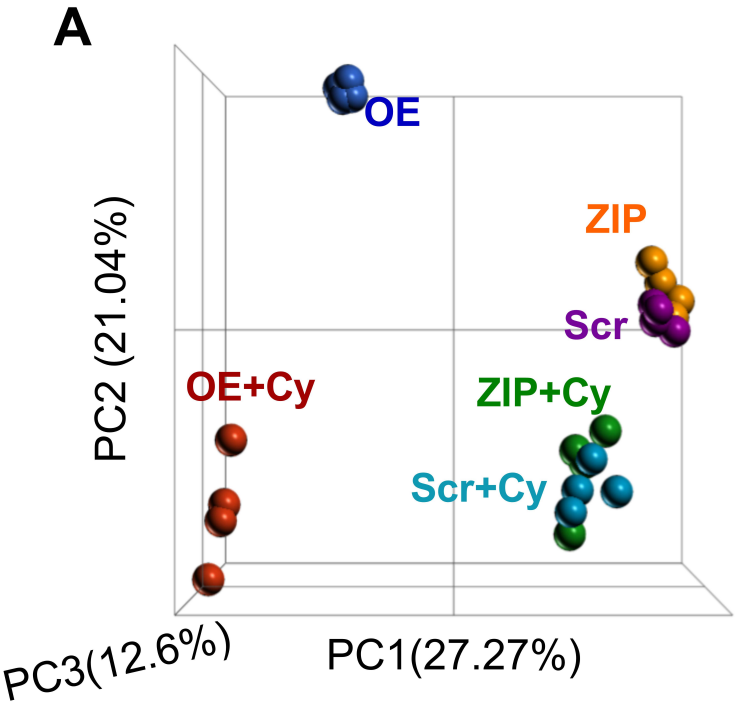
A
OE
ZIP
Scr
OE+Cy
ZIP+Cy
Scr+Cy
PC2 (21.04%)
PC3(12.6%)
PC1(27.27%)

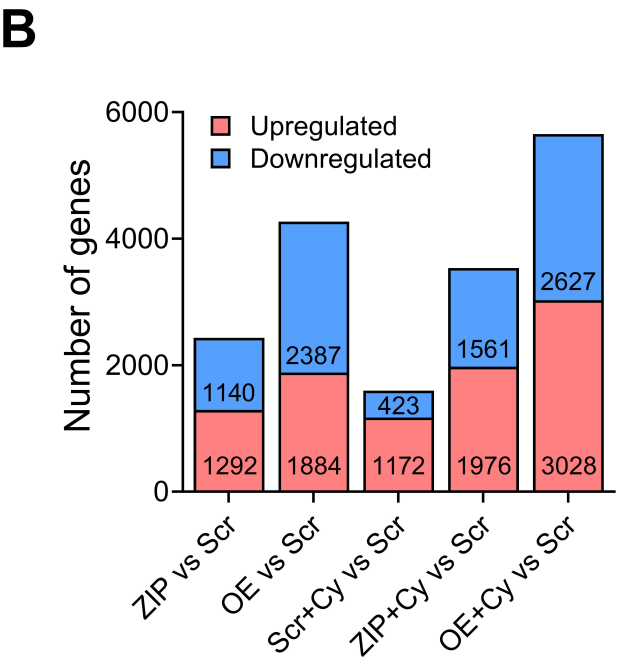
B
Upregulated
Downregulated
Number of genes
6000
4000
2000
0
1140
1292
2387
1884
423
1172
1561
1976
2627
3028
ZIP vs Scr
OE vs Scr
Scr+Cy vs Scr
ZIP+Cy vs Scr
OE+Cy vs Scr

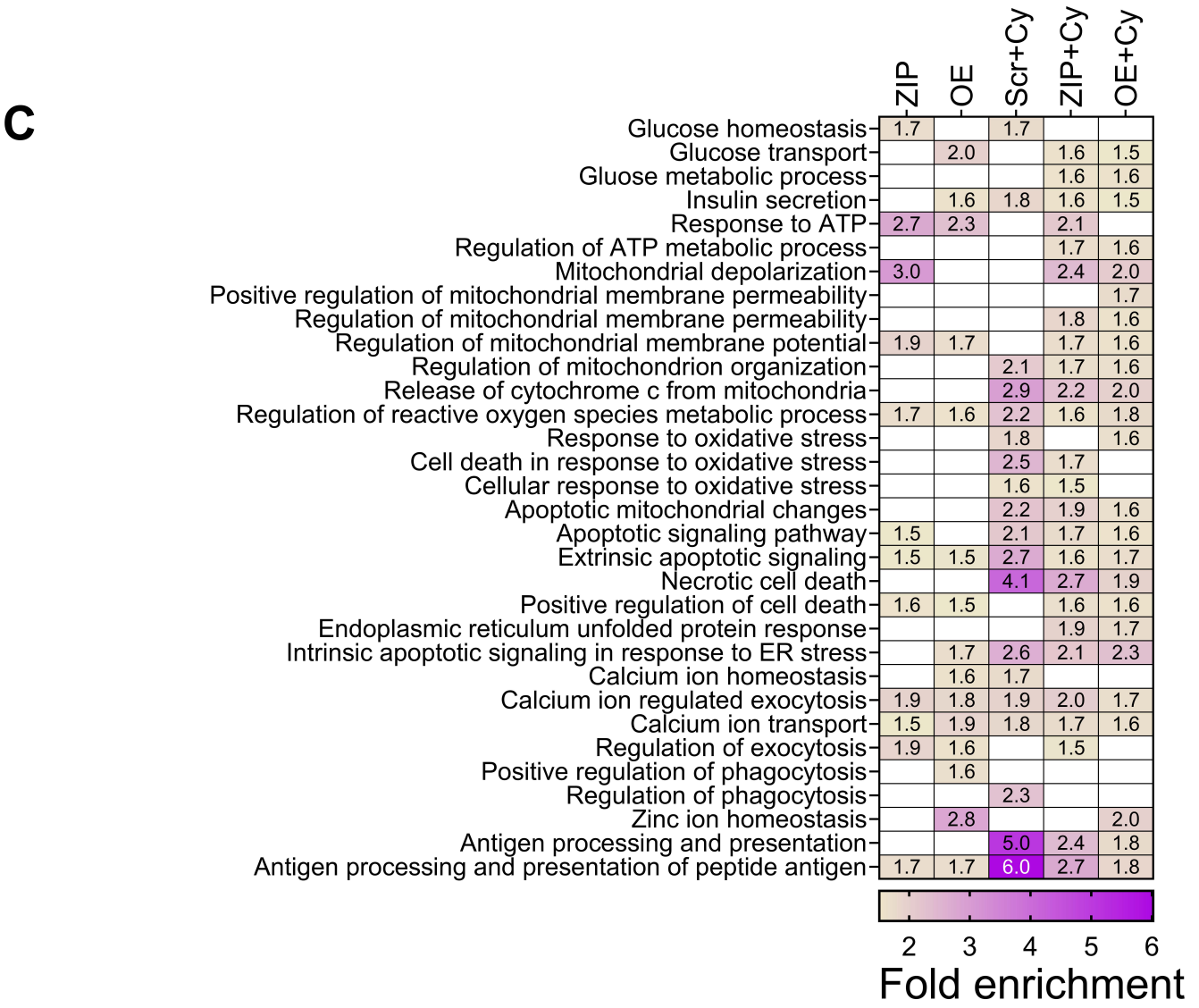
C
ZIP
OE
Scr+Cy
ZIP+Cy
OE+Cy
Glucose homeostasis 1.7 1.7
Glucose transport 2.0 1.6 1.5
Gluose metabolic process 1.6 1.6
Insulin secretion 1.6 1.8 1.6 1.5
Response to ATP 2.7 2.3 2.1
Regulation of ATP metabolic process 1.7 1.6
Mitochondrial depolarization 3.0 2.4 2.0
Positive regulation of mitochondrial membrane permeability 1.7
Regulation of mitochondrial membrane permeability 1.8 1.6
Regulation of mitochondrial membrane potential 1.9 1.7 1.7 1.6
Regulation of mitochondrion organization 2.1 1.7 1.6
Release of cytochrome c from mitochondria 2.9 2.2 2.0
Regulation of reactive oxygen species metabolic process 1.7 1.6 2.2 1.6 1.8
Response to oxidative stress 1.8 1.6
Cell death in response to oxidative stress 2.5 1.7
Cellular response to oxidative stress 1.6 1.5
Apoptotic mitochondrial changes 2.2 1.9 1.6
Apoptotic signaling pathway 1.5 2.1 1.7 1.6
Extrinsic apoptotic signaling 1.5 1.5 2.7 1.6 1.7
Necrotic cell death 4.1 2.7 1.9
Positive regulation of cell death 1.6 1.5 1.6 1.6
Endoplasmic reticulum unfolded protein response 1.9 1.7
Intrinsic apoptotic signaling in response to ER stress 1.7 2.6 2.1 2.3
Calcium ion homeostasis 1.6 1.7
Calcium ion regulated exocytosis 1.9 1.8 1.9 2.0 1.7
Calcium ion transport 1.5 1.9 1.8 1.7 1.6
Regulation of exocytosis 1.9 1.6 1.5
Positive regulation of phagocytosis 1.6
Regulation of phagocytosis 2.3
Zinc ion homeostasis 2.8 2.0
Antigen processing and presentation 5.0 2.4 1.8
Antigen processing and presentation of peptide antigen 1.7 1.7 6.0 2.7 1.8
2 3 4 5 6
Fold enrichment

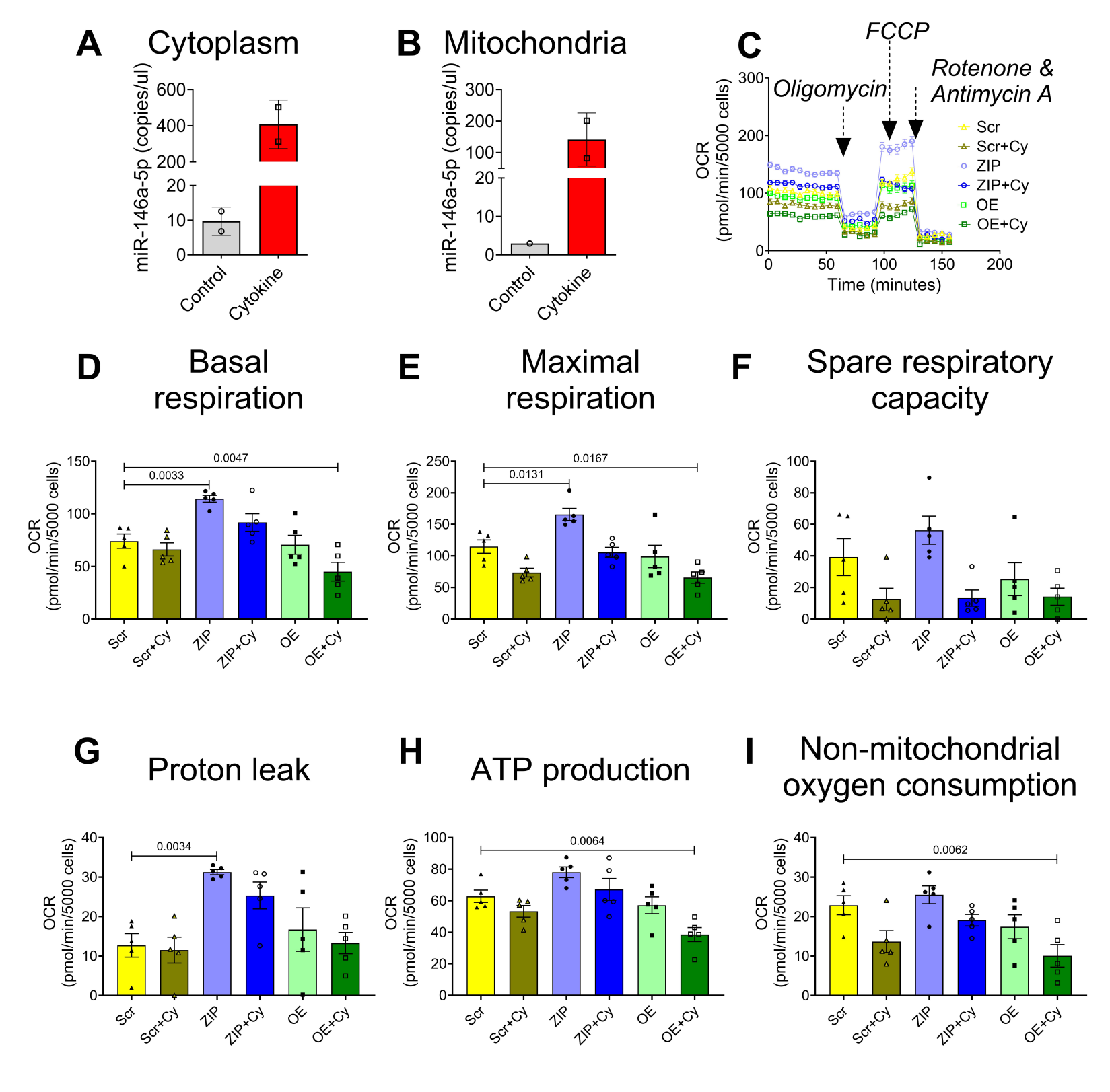
A
Cytoplasm
miR-146a-5p (copies/ul)
600
400
200
20
10
0
Control
Cytokine
B
Mitochondria
miR-146a-5p (copies/ul)
300
200
100
20
10
0
Control
Cytokine
C
FCCP
Oligomycin
Rotenone &
Antimycin A
OCR
(pmol/min/5000 cells)
300
200
100
0
0
50
100
150
200
Time (minutes)
Scr
Scr+Cy
ZIP
ZIP+Cy
OE
OE+Cy
D
Basal
respiration
OCR
(pmol/min/5000 cells)
150
100
50
0
0.0047
0.0033
Scr
Scr+Cy
ZIP
ZIP+Cy
OE
OE+Cy
E
Maximal
respiration
OCR
(pmol/min/5000 cells)
250
200
150
100
50
0
0.0167
0.0131
Scr
Scr+Cy
ZIP
ZIP+Cy
OE
OE+Cy
F
Spare respiratory
capacity
OCR
(pmol/min/5000 cells)
100
80
60
40
20
0
Scr
Scr+Cy
ZIP
ZIP+Cy
OE
OE+Cy
G
Proton leak
OCR
(pmol/min/5000 cells)
40
30
20
10
0
0.0034
Scr
Scr+Cy
ZIP
ZIP+Cy
OE
OE+Cy
H
ATP production
OCR
(pmol/min/5000 cells)
100
80
60
40
20
0
0.0064
Scr
Scr+Cy
ZIP
ZIP+Cy
OE
OE+Cy
I
Non-mitochondrial
oxygen consumption
OCR
(pmol/min/5000 cells)
40
30
20
10
0
0.0062
Scr
Scr+Cy
ZIP
ZIP+Cy
OE
OE+Cy

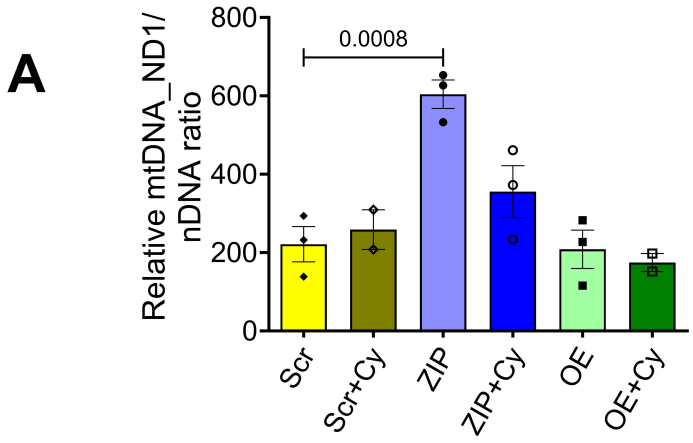
A
Relative mtDNA_ND1/
nDNA ratio
800
600
400
200
0
0.0008
Scr
Scr+Cy
ZIP
ZIP+Cy
OE
OE+Cy

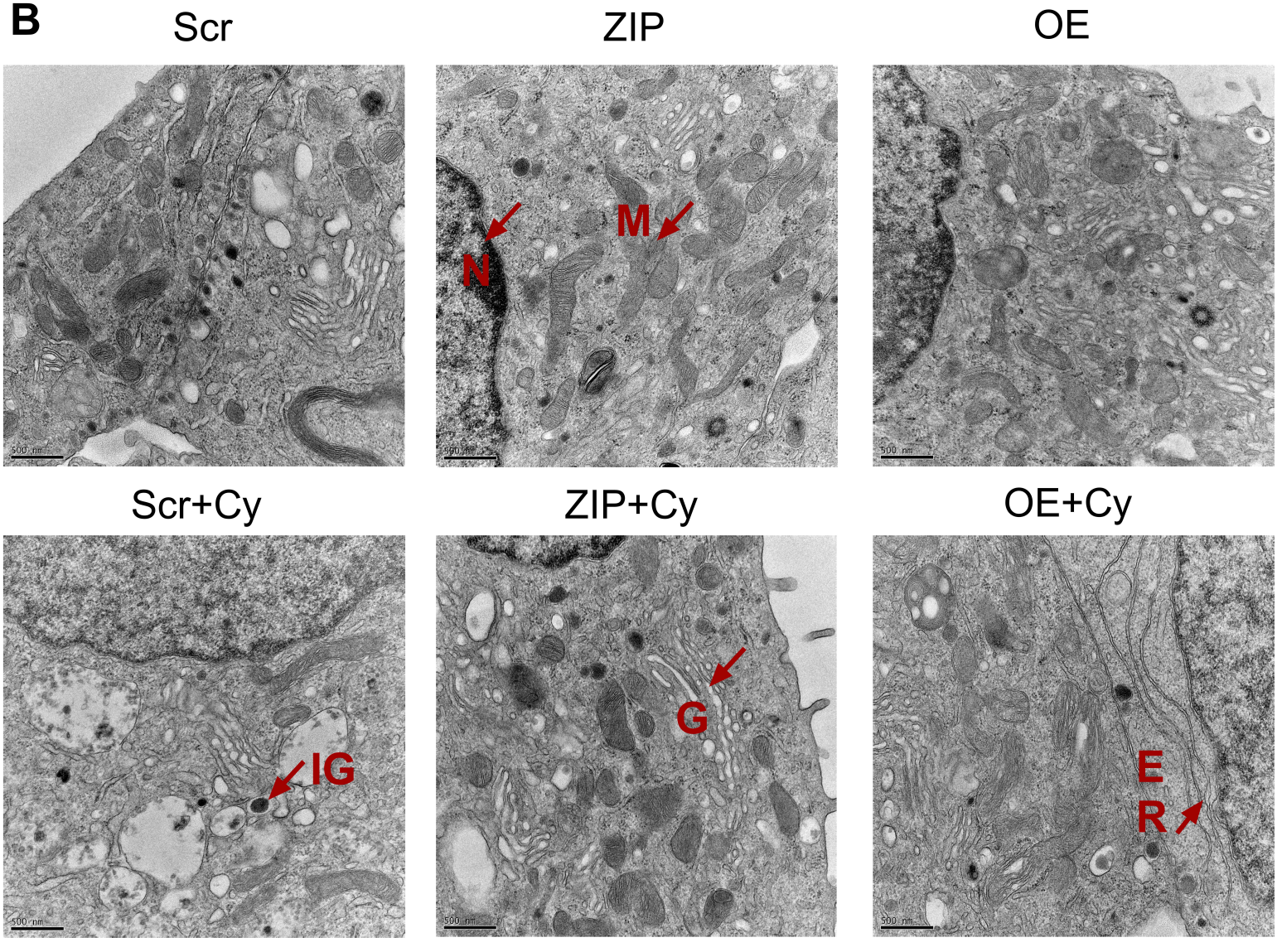
B
Scr
ZIP
OE
N
M
Scr+Cy
ZIP+Cy
OE+Cy
IG
G
E
R

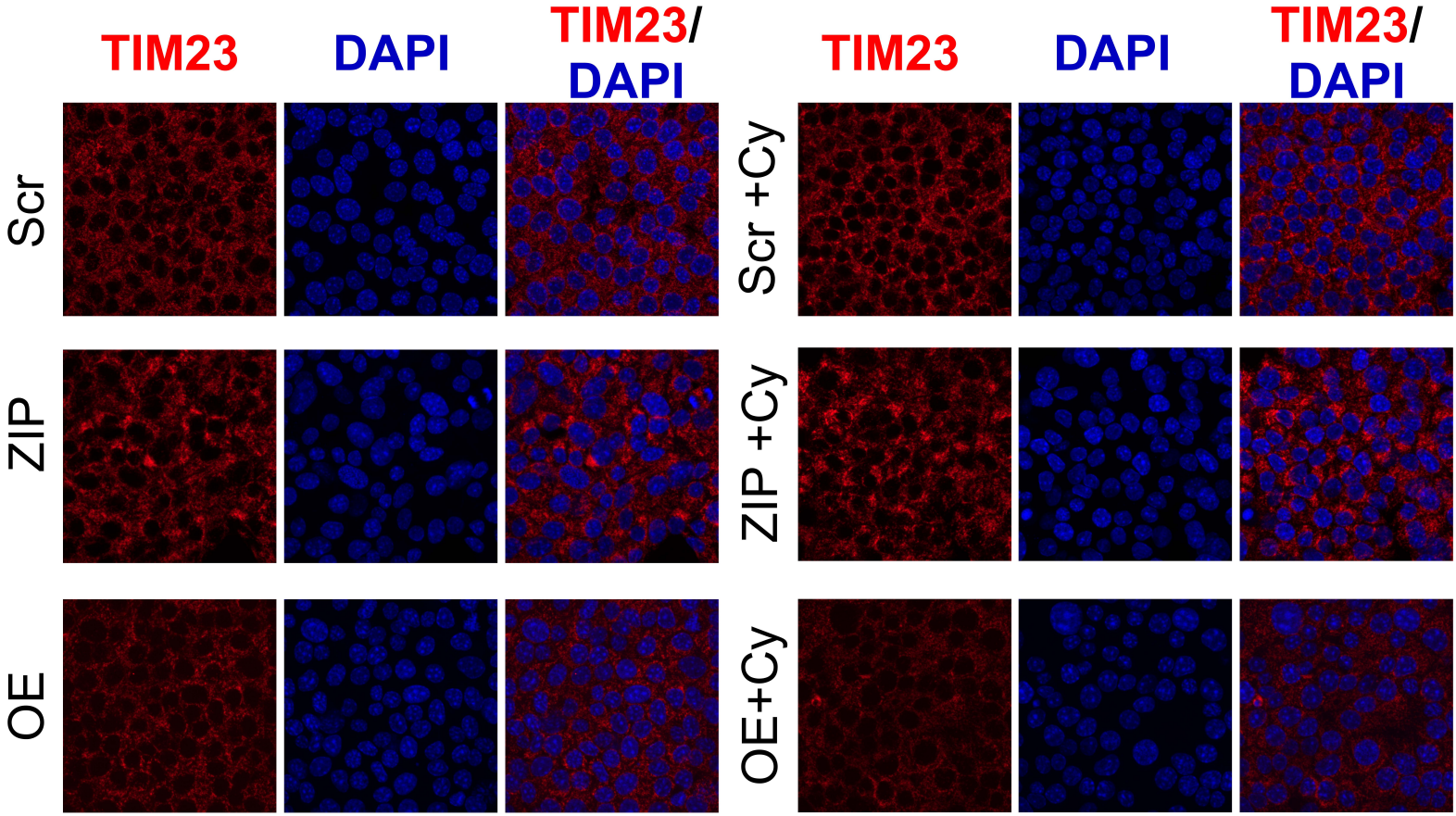
TIM23
DAPI
TIM23/ DAPI
TIM23
DAPI
TIM23/ DAPI
Scr
Scr +Cy
ZIP
ZIP +Cy
OE
OE+Cy

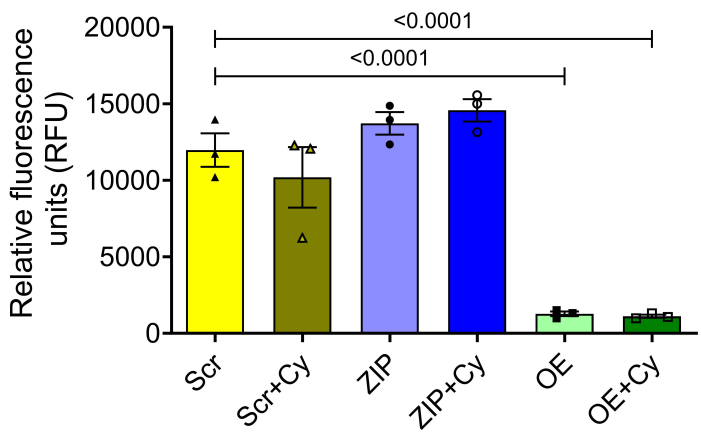
Relative fluorescence units (RFU)
20000
15000
10000
5000
0
<0.0001
<0.0001
Scr
Scr+Cy
ZIP
ZIP+Cy
OE
OE+Cy

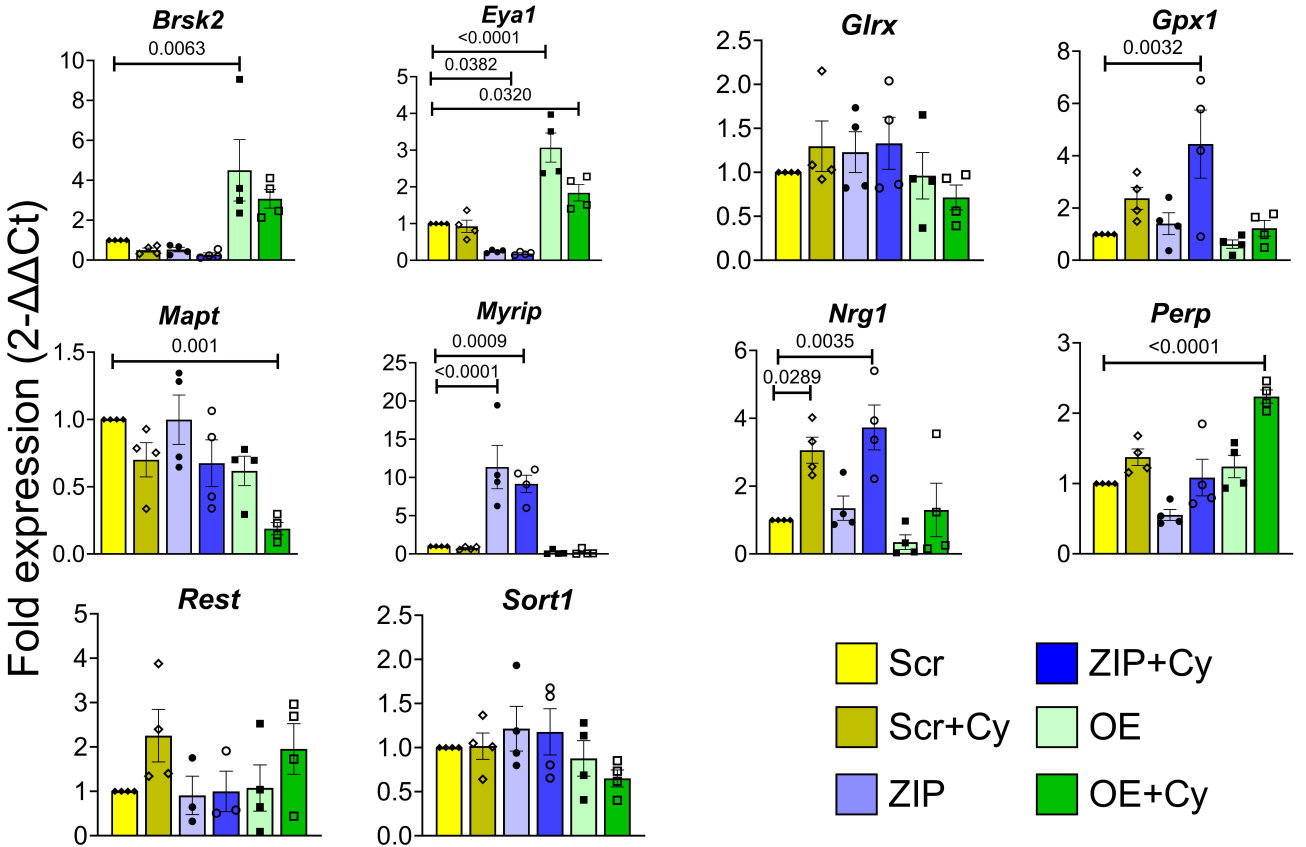
Fold expression (2-ΔΔCt)
Brsk2
0.0063
Eya1
<0.0001
0.0382
0.0320
Glrx
Gpx1
0.0032
Mapt
0.001
Myrip
0.0009
<0.0001
Nrg1
0.0035
0.0289
Perp
<0.0001
Rest
Sort1
Scr
Scr+Cy
ZIP
ZIP+Cy
OE
OE+Cy

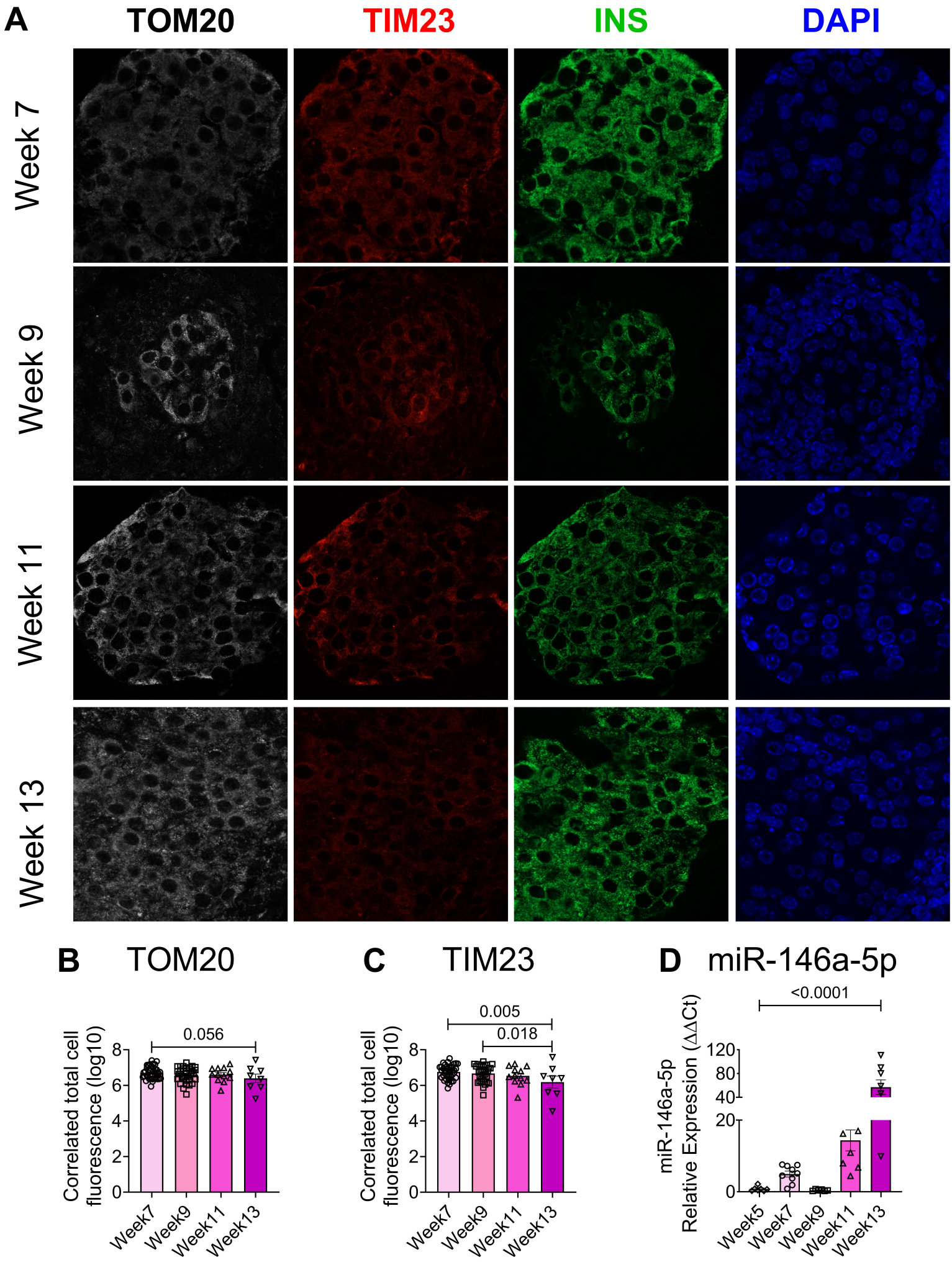
A
TOM20
TIM23
INS
DAPI
Week 7
Week 9
Week 11
Week 13
B
TOM20
Correlated total cell fluorescence (log10)
0.056
Week7
Week9
Week11
Week13
C
TIM23
Correlated total cell fluorescence (log10)
0.005
0.018
Week7
Week9
Week11
Week13
D
miR-146a-5p
miR-146a-5p Relative Expression (ΔΔCt)
<0.0001
Week5
Week7
Week9
Week11
Week13

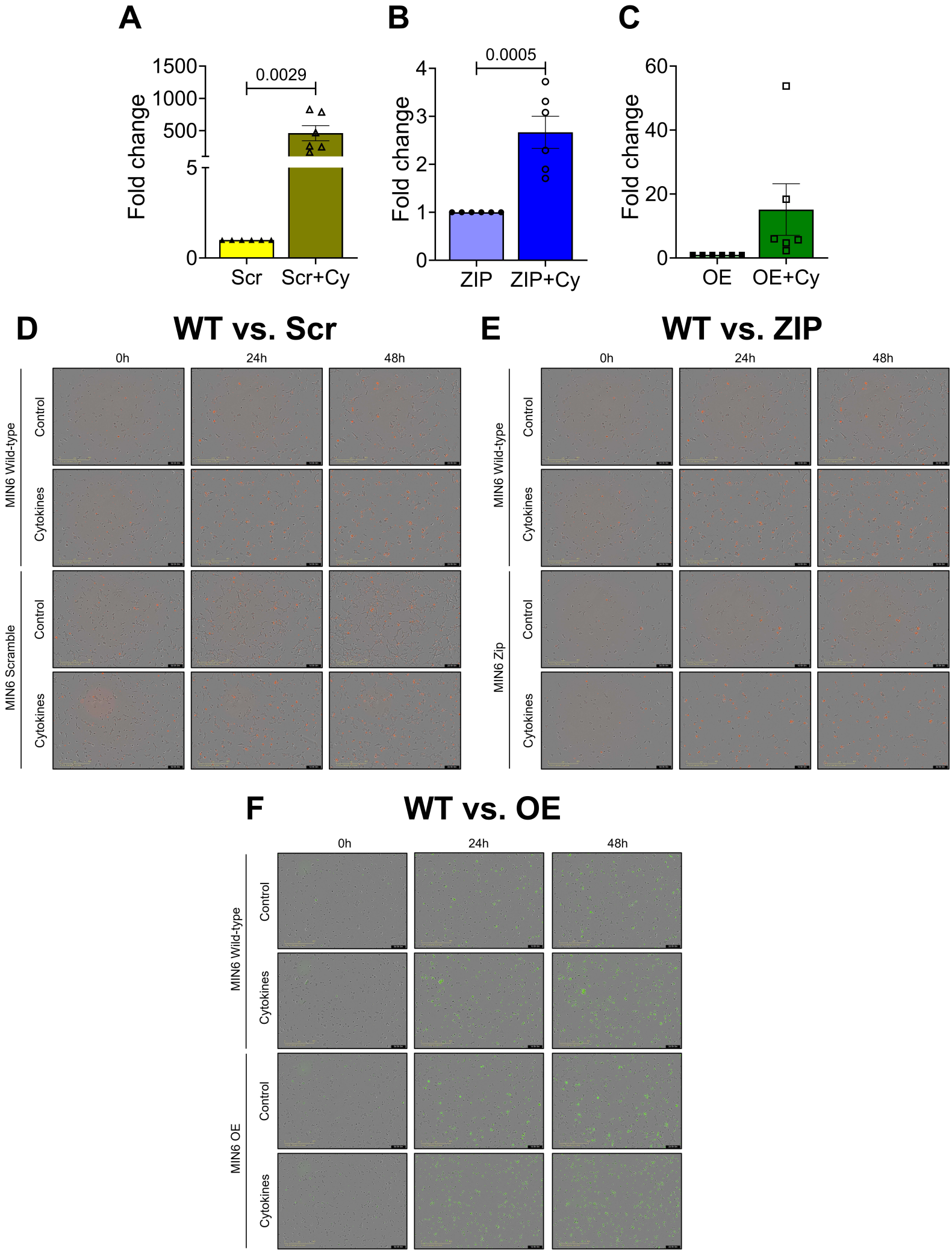
A
Fold change
1500
1000
500
5
0
0.0029
Scr
Scr+Cy
B
Fold change
4
3
2
1
0
0.0005
ZIP
ZIP+Cy
C
Fold change
60
40
20
0
OE
OE+Cy
D
WT vs. Scr
0h
24h
48h
MIN6 Wild-type
Control
Cytokines
MIN6 Scramble
Control
Cytokines
E
WT vs. ZIP
0h
24h
48h
MIN6 Wild-type
Control
Cytokines
MIN6 Zip
Control
Cytokines
F
WT vs. OE
0h
24h
48h
MIN6 Wild-type
Control
Cytokines
MIN6 OE
Control
Cytokines

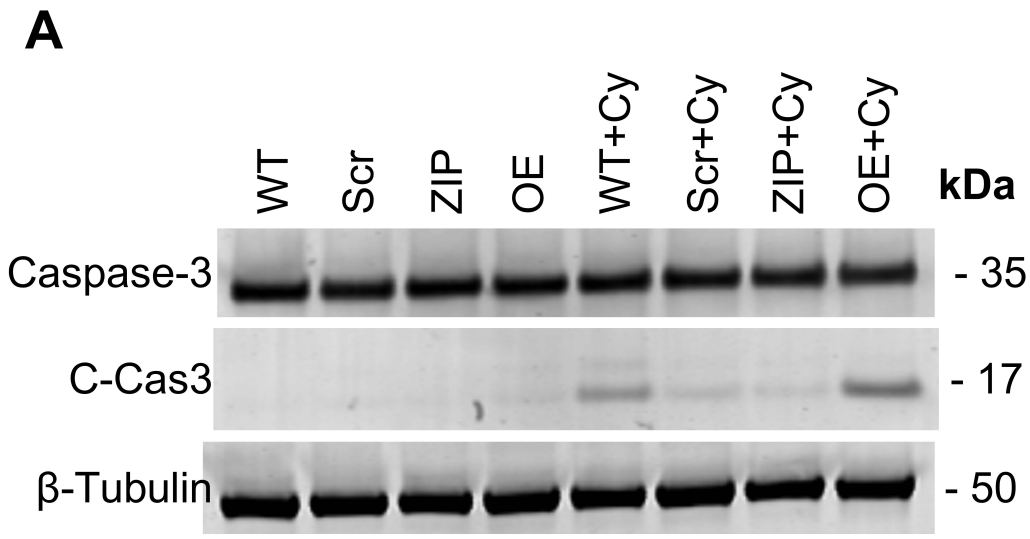
A
WT
Scr
ZIP
OE
WT+Cy
Scr+Cy
ZIP+Cy
OE+Cy
kDa
Caspase-3
- 35
C-Cas3
- 17
β-Tubulin
- 50

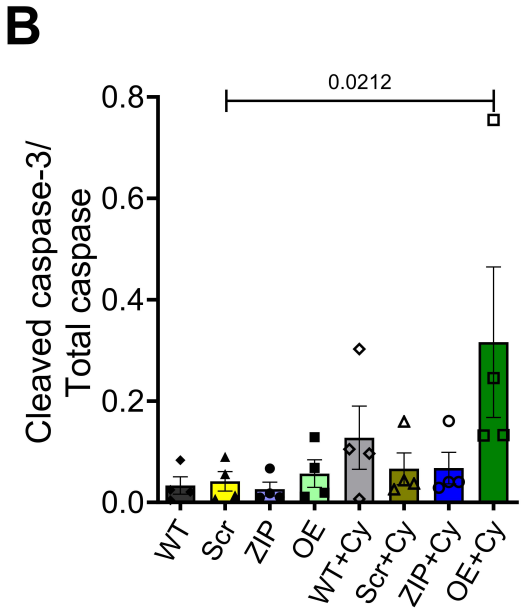
B
0.0212
Cleaved caspase-3/
Total caspase
0.8
0.6
0.4
0.2
0.0
WT
Scr
ZIP
OE
WT+Cy
Scr+Cy
ZIP+Cy
OE+Cy

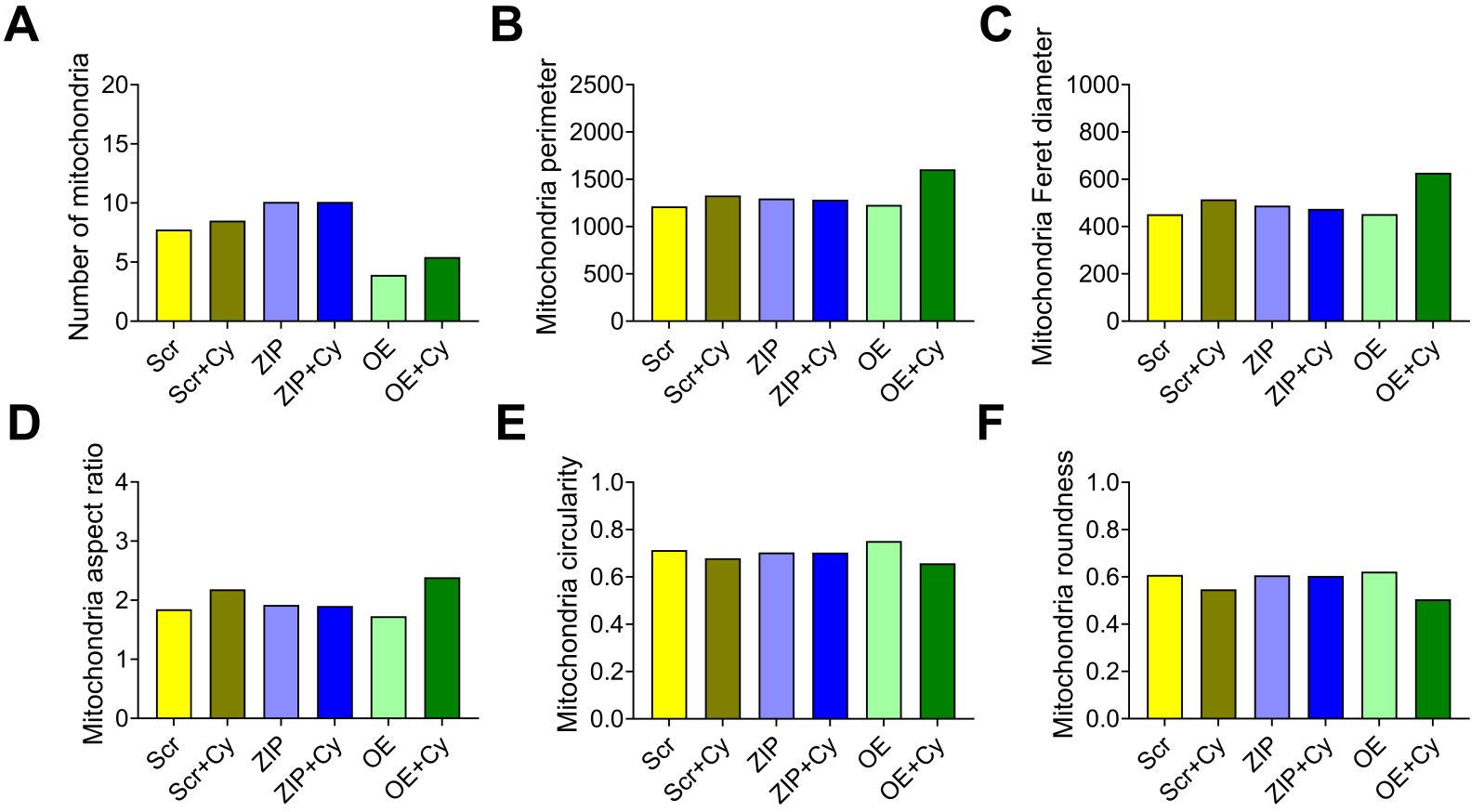
A
Number of mitochondria
20
15
10
5
0
Scr
Scr+Cy
ZIP
ZIP+Cy
OE
OE+Cy
B
Mitochondria perimeter
2500
2000
1500
1000
500
0
Scr
Scr+Cy
ZIP
ZIP+Cy
OE
OE+Cy
C
Mitochondria Feret diameter
1000
800
600
400
200
0
Scr
Scr+Cy
ZIP
ZIP+Cy
OE
OE+Cy
D
Mitochondria aspect ratio
4
3
2
1
0
Scr
Scr+Cy
ZIP
ZIP+Cy
OE
OE+Cy
E
Mitochondria circularity
1.0
0.8
0.6
0.4
0.2
0.0
Scr
Scr+Cy
ZIP
ZIP+Cy
OE
OE+Cy
F
Mitochondria roundness
1.0
0.8
0.6
0.4
0.2
0.0
Scr
Scr+Cy
ZIP
ZIP+Cy
OE
OE+Cy